Continuous and discrete modeling of failure in geomaterials

Félix Darve, Cédric Lambert

Continuous and discrete modelling of failure in geomechanics

Félix Darve* and Cédric Lambert*

* Laboratoire Sols, Solides, Structures, RNVO, Alert Geomaterials, INPG, UJF, CNRS, Grenoble, France

Abstract Practice shows that there are various modes of failure in geomaterials. Different criteria have been proposed to analyse these failures. Hill's Condition of Stability and diffuse modes of failure are particularly considered in this paper in a dual framework : continuum mechanics and discrete mechanics. With the assumption of continuous media and as an illustration, the experiments have shown that q-constant loading paths can exhibit non-localized failure modes and they are analyzed by the second order work criterion. More generally, the equations of the boundaries of the unstable domain and of the cones of unstable stress directions are established in axisymmetric and plane strain conditions. With the assumption of discrete media, grain avalanches are considered and, spatial and temporal correlations between bursts of kinetic energy and peaks of negative values of second order work are exhibited from discrete computations. It is concluded that the second order work criterion (under its double form : continuous and discrete) can be a proper tool to analyse diffuse modes of failure in geomaterials.

1 Introduction

One of the most basic question in geomechanics is how to define, analyse and simulate failure. The general way to introduce the phenomenon of failure is to note that in elementary laboratory experiments, some loading paths are leading to limit stress states. Along these paths, these stress states can not be passed : experimentally they constitute asymptotical limit states.
By restricting our study to elasto-plastic behaviors, the general expression of rate-independent constitutive equations is given by :

$$d\sigma_{ij} = L_{ijkl} d\varepsilon_{kl} \tag{1.1}$$

where the elasto-plastic tangent operator $\underset{\sim}{L}$ depends on the previous stress-strain history (characterized by state variables and memory parameters χ) and on the direction of $\underset{\sim}{d\varepsilon}$ (characterized by unit matrix $\underset{\sim}{v} = \underset{\sim}{d\varepsilon}/\|\underset{\sim}{d\varepsilon}\|$).
In the six-dimensional associated spaces it comes :

$$d\sigma_\alpha = N_{\alpha\beta}(v_\gamma) d\varepsilon_\beta \qquad (\alpha, \beta = 1, \ldots, 6) \tag{1.2}$$

$v_\gamma = d\varepsilon_\gamma / \|\underset{\sim}{d\varepsilon}\|$ and $\|\underset{\sim}{d\varepsilon}\| = \sqrt{d\varepsilon_\alpha d\varepsilon_\alpha}$.
From a mathematical point of view, limit stress points are characterized by :

$$\underset{\sim}{d\sigma} = \underset{\sim}{0} \qquad \text{with} \qquad \|\underset{\sim}{d\varepsilon}\| \neq 0 \tag{1.3}$$

Condition (1.3) implies :

$$\det \underset{\sim}{N}_\chi (\underset{\sim}{v}) = 0 \qquad \text{and} \qquad \underset{\sim}{N}_\chi (\underset{\sim}{v}) \underset{\sim}{d\varepsilon} = 0 \tag{1.4}$$

If the constitutive relation is incrementally linear, $\underset{\sim}{N}$ is independent on $\underset{\sim}{v}$. The first equation of (1.4) represents precisely the plastic limit criterion because this is the equation of an hyper-surface in the six-dimensional stress space. The second equation represents the material flow rule, since this equation gives the direction of $\underset{\sim}{d\varepsilon}$ when the plastic limit surface has been reached.
For incrementally piecewise linear constitutive relations, where $\underset{\sim}{N}$ depends in a discontinuous manner from $\underset{\sim}{v}$ (inside "tensorial zones", see the chapter by Darve and Servant), $\det \underset{\sim}{N}_\chi (\underset{\sim}{v}) = 0$ is still the equation of an hyper-surface in the stress space, possibly involving several plastic mechanisms. Besides, $\underset{\sim}{N}_\chi (\underset{\sim}{v}) \underset{\sim}{d\varepsilon} = 0$ is a singular generalized flow rule with vertices which are locally constituted by pyramids (Hill R. , 1967).
This classical elasto-plastic view of failure has given rise to the wide domain of the "limit analysis", where the whole body at a failure state is assumed to have reached the plastic limit condition.
However, in practice, various modes of failure are encountered : localized modes in shear bands (Rice J.R. , 1976; Vardoulakis I. & Sulem J. , 1995; Darve F. , 1984), in compaction bands or in dilation bands, diffuse modes due to geometric instabilities (buckling,...) or with a chaotic displacement field,...For non-associated materials (essentially because of the non-symmetry of the elasto-plastic matrix $\underset{\sim}{N}$), the elasto-plastic theory shows effectively that, by considering proper bifurcation criteria, these localized or diffuse modes of failure can appear before the plastic limit condition (Bigoni D. & Hueckel T. , 1991).
In relation with these various modes of failure, different bifurcation criteria are available. With respect to shear band formation by plastic strain localizations, Rice's criterion (1976) based on the description of such an incipient shear band of normal n corresponds to vanishing values of the so-called "acoustic tensor" :

$$\det({}^t n \underset{\sim}{L} n) = 0 \tag{1.5}$$

For non-associated materials, equation (1.5) can be satisfied before plasticity criterion (1.4). This has been verified experimentally for dense sand (Desrues J. , 1990). Strain localization corresponds to a bifurcation of the strain mode from a diffuse one to a strictly discontinuous one. This kind of bifurcation can be called "discontinuous bifurcation".
"Continuous bifurcations" (Darve F. & Roguiez X. , 1998) opposed to the previous one correspond also to a failure mode, but without strain localization. Such failure mode is called "diffuse failure" and this is the response path which is subjected to a bifurcation

with a loss of constitutive uniqueness at the bifurcation point. According to the control mode (stress, strain or mixed control) of the loading path, different response paths are possible from the bifurcation point. For certain control modes, the loading is no more "controllable" in Nova's sense (Nova R. , 1994).
These continuous bifurcations and the related diffuse modes of failure can be detected by Hill's sufficient condition of stability (Hill R. , 1958) which corresponds, for unstable states, to vanishing values of second order work, that is to say vanishing values of the determinant of the symmetric part of matrix $\underset{\sim}{N}$ for incrementally linear constitutive relations. Section 2 of this chapter is devoted to recall briefly Lyapunov's definition of stability (Lyapunov A.M. , 1907) and Hill's condition, then to apply them to the well known case of the failure of undrained loose sands. The generalization to axisymmetric paths and to plane strain conditions allows to determine numerically and analytically the "unstable" domain (i.e. the failure domain) and, inside this domain, the "unstable" stress directions which form cones for both these cases.
In section 3, this analysis is applied to axisymmetric q-constant loading path, since some experiments (Chu J. & Leong W.K. (2003)) have shown failure modes without localization along these paths in the case of loose sands.
Section 2 and 3 have illustrated the application of Hill's condition in the framework of continuum mechanics. It is also possible to consider a discrete form of second order work (Mandel J. , 1966) and to apply it to boundary value problems described by discrete mechanics. In this perspective the most known examples of typical failures are the so-called "grain avalanches". This phenomenon has been extensively studied specially by physicists of granular media (see Hermann H.J. et al. (1998) for example). It has been also considered as a paradigm for the concept of "self-organized criticality" (Bak P. , 1996). In section 4 of this paper, grain avalanches are analyzed in the strict framework of discrete mechanics. The, more or less local, failures will be characterized by bursts of kinetic energy (computed by a discrete element method). Strong spatial and temporal correlations between these bursts and the peaks of negative values of second order work are exhibited. These results represent another illustration of the deep link which relates certain failure modes and second order work, which could constitute a novel indicator of failure.

2 Material instabilities

The most basic definition of stability was certainly proposed by Lyapunov A.M. (1907). Applied to the field of continuum mechanics it states that :
"A stress-strain state, for a given material after a given loading history, is called stable, if for every positive scalar ε, a positive number $\eta(\varepsilon)$ exists such that for all incremental loading bounded by η, the associated responses remain bounded by ε"
According to this definition, all limit stress states (as defined in the introduction) are unstable.
Indeed if a "small" incremental reverse stress from a limit stress state is considered, a "small" (more or less elastic) response will be induced, while a "small" incremental additional stress beyond the limit state produces a "large" strain response. Lyapunov's

definition of stability is interesting because it states clearly that material instabilities can be conjectured in elasto-plastic media. Since some limit stress states are strictly inside Mohr-Coulomb plastic limit surface (because of non-associativity) - an example is given in section 2.1 - some instabilities can be expected before reaching Mohr-Coulomb plastic limit condition.
But, even if this first conclusion is essential, Lyapunov's definition is not a proper tool to investigate instabilities in geomaterials. For that, we are now considering Hill's sufficient condition of stability (Hill R. , 1958). According to Hill, a stress-strain state is unstable if it exists at least one loading direction which can be pursued in an infinitesimal manner without any input of energy from outside. In practice it means that the deformation process will continue "on one's own" under dead loads . Indeed, in some situations, failure needs some energy from outside of soil boby (for example, the weight of a structure on a foundation), while in other situations energy is not needed (landslides, rockfalls,...).
Finally Hill's condition of stability states that a stress-strain state is stable if, for all $(d\underset{\sim}{\sigma}, d\underset{\sim}{\varepsilon})$ linked by the constitutive relation, the second order work is strictly positive :

$$d^2W = d\underset{\sim}{\sigma}\, d\underset{\sim}{\varepsilon} > 0 \tag{2.1}$$

For hyperelastic-plastic constitutive relations, Drucker's postulate ($d\underset{\sim}{\sigma}\, d\underset{\sim}{\varepsilon}^p > 0$, see Drucker D.C. (1959)) implies Hill's condition, since : $d\underset{\sim}{\sigma}\, d\underset{\sim}{\varepsilon}^e \geq 0$ in hyperelasticity, and : $d\underset{\sim}{\sigma}\, d\underset{\sim}{\varepsilon} = d\underset{\sim}{\sigma}\, d\underset{\sim}{\varepsilon}^e + d\underset{\sim}{\sigma}\, d\underset{\sim}{\varepsilon}^p$, with the usual decomposition of the incremental strain into an elastic part and a plastic part in classical elasto-plasticity.
The link between Lyapunov's definition and Hill's condition has not been established in a general manner. The equivalence has been proved by Koïter W.T. (1969) in the case of elasticity. If the equivalence between Lyapunov's definition and "non-controllable" paths in Nova's sense (Nova R. , 1994) is accepted, then non-controllability and Hill's condition are equivalent in classical elasto-plasticity (Nova R. , 1994). For hypoplastic relations (as defined by Chambon R. et al. (1994)) the positiveness of second order work assures the uniqueness (Chambon R. & Caillerie D. , 1999). In the general case of incrementally non-linear constitutive relations, counter-example might exist. In the next sub-section, all that is illustrated by the well known case of the undrained triaxial behavior of loose sands.

2.1 Undrained paths on loose sands

The undrained triaxial behavior of loose sands is typically represented in figure 1, where q is passing through a maximum which is situated strictly inside Mohr-Coulomb plastic limit surface. The experiments show that, if a "small" additional axial force is applied at q peak, there is a sudden failure of the whole sample without any localization pattern. Because of this sudden failure for a small perturbation at q peak, q peak is an unstable state according to Lyapunov's definition.
For axisymmetric conditions and coinciding principal axes, the second order work is equal to :

$$d^2W = d\sigma_1 d\varepsilon_1 + 2d\sigma_3 d\varepsilon_3 \tag{2.2}$$

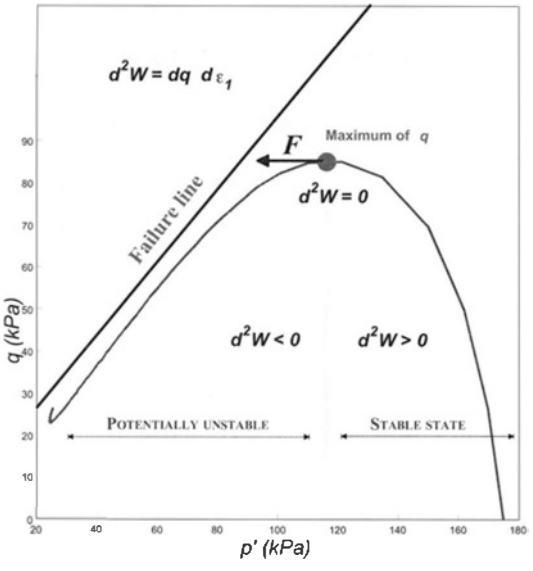

Figure 1. Example of an unstable state related to a diffuse mode of failure strictly inside Mohr-Coulomb plastic limit condition : typical undrained triaxial behavior of a loose sand.

and with the isochoric condition : $d\varepsilon_1 + 2d\varepsilon_3 = 0$, it comes :

$$d^2W = dqd\varepsilon_1 \qquad \text{with :} \qquad q = \sigma_1 - \sigma_3 \tag{2.3}$$

Thus according to Hill's condition , q peak has to be considered as an unstable state ((Darve F. & Chau B. , 1987)).
Let us see now that we can define at q peak a generalized plasticity criterion and a generalized flow rule (as defined in equation (1.4)).
Because $q - \varepsilon_1$ and $\varepsilon_v - \varepsilon_3$ (with : $\varepsilon_v = \varepsilon_1 + 2\varepsilon_3$) are conjugate variables with respect to energy : $\sigma_1\varepsilon_1 + 2\sigma_3\varepsilon_3 \equiv q\varepsilon_1 + \varepsilon_v\sigma_3$, the constitutive relation can be written under the following form :

$$\begin{bmatrix} dq \\ d\varepsilon_v \end{bmatrix} = \underset{\sim}{P} \begin{bmatrix} d\varepsilon_1 \\ d\sigma_3 \end{bmatrix} \tag{2.4}$$

For an undrained loading, the isochoric condition is fulfilled, thus :

$$d\varepsilon_v = 0 \tag{2.5}$$

As dq is vanishing at q peak, it comes :

$$\det \underset{\sim}{P} = 0 \qquad \text{and} \qquad \underset{\sim}{P} \begin{bmatrix} d\varepsilon_1 \\ d\sigma_3 \end{bmatrix} = \begin{bmatrix} 0 \\ 0 \end{bmatrix} \tag{2.6}$$

These relations generalize equations (1.4). The failure mode can be viewed as the eigenmode associated to the vanishing eigenvalue of matrix $\underset{\sim}{P}$.

In conclusion it is emphasized that q peak is a proper failure state (satisfying all the criteria associated to the notion of failure) which is situated strictly inside Mohr-Coulomb plastic limit surface and is related to a diffuse mode of failure.
In several previous papers (Darve F. & Laouafa F. , 2000, 2001; Laouafa F. & Darve F. , 2001) we have exhibited numerically the boundaries of the unstable domain in axisymmetric conditions, in plane strain conditions and more generally for 3D conditions. Besides, second order work is typically a directional quantity in the stress space. Indeed, if the constitutive relation is given by :

$$\underset{\sim}{d\varepsilon} = \underset{\sim}{\underset{\sim}{M}}(\underset{\sim}{u})\underset{\sim}{d\sigma} \qquad \text{with} \qquad \underset{\sim}{u} = \underset{\sim}{d\sigma}/\|\underset{\sim}{d\sigma}\| \tag{2.7}$$

it comes : $d^2W = {}^t\underset{\sim}{d\sigma}\,\underset{\sim}{d\varepsilon} = {}^t\underset{\sim}{d\sigma}\,\underset{\sim}{\underset{\sim}{M}}(\underset{\sim}{u})\underset{\sim}{d\sigma}$ or, by dividing by $\|\underset{\sim}{d\sigma}\|^2$:

$$d^2W/\|\underset{\sim}{d\sigma}\|^2 = {}^t\underset{\sim}{u}\,\underset{\sim}{\underset{\sim}{M}}(\underset{\sim}{u})\underset{\sim}{u} \tag{2.8}$$

Thus there are cones of unstable stress directions, where the second order work takes negative values.
Next sub-section 2.2 is devoted to the analytical determination of the equations of the unstable domain and of the cones of unstable stress directions in the case of an incrementally piecewise linear constitutive relation for axisymmetric conditions.

2.2 Axisymmetric loading paths

Analytical explicit computations are feasible with our incrementally piecewise linear model,called "the octo-linear model" (see chapter 1 by Darve and Servant and (Darve F. & Labanieh S. , 1982)) because it is constituted by 8 linear relations between $\underset{\sim}{d\varepsilon}$ and $\underset{\sim}{d\sigma}$ in 8 "tensorial zones". Let us restrict the presentation to the axisymmetric case with 4 tensorial zones. In such a case, the expression of the model is given by :

$$\begin{bmatrix} d\varepsilon_1 \\ \sqrt{2}d\varepsilon_3 \end{bmatrix} = \frac{1}{2}\left(\underset{\sim}{Q}^+ + \underset{\sim}{Q}^-\right)\begin{bmatrix} d\sigma_1 \\ \sqrt{2}d\sigma_3 \end{bmatrix} + \frac{1}{2}\left(\underset{\sim}{Q}^+ - \underset{\sim}{Q}^-\right)\begin{bmatrix} |d\sigma_1| \\ \sqrt{2}|d\sigma_3| \end{bmatrix} \tag{2.9}$$

with :

$$\underset{\sim}{Q}^{\pm} = \begin{bmatrix} \frac{1}{E_1^{\pm}} & -\sqrt{2}\frac{V_3^{1\pm}}{E_3^{\pm}} \\ -\sqrt{2}\frac{V_1^{3\pm}}{E_1^{\pm}} & \frac{1-V_3^{3\pm}}{E_3^{\pm}} \end{bmatrix} \tag{2.10}$$

where index (+) means "compression" ($d\sigma_i > 0$) and (-) "extension" ($d\sigma_i < 0$) in the axial direction "i" of "generalized" triaxial paths (two lateral constant stresses σ_j and σ_k). E_i are "generalized" tangent Young moduli and V_i^j "generalized" tangent Poisson's ratios defined by :

$$E_i = \left(\frac{\partial\sigma_i}{\partial\varepsilon_i}\right)_{\sigma_j,\sigma_k} ; V_i^j = -\left(\frac{\partial\varepsilon_j}{\partial\varepsilon_i}\right)_{\sigma_j,\sigma_k} ; V_i^k = -\left(\frac{\partial\varepsilon_k}{\partial\varepsilon_i}\right)_{\sigma_j,\sigma_k}$$

According to the signs of $d\sigma_1$ and $d\sigma_3$ (4 possibilities), there are 4 linear relations between $\underset{\sim}{d\varepsilon}$ and $\underset{\sim}{d\sigma}$, (see details in chapter 1).

In order to investigate the sign of second order work at a given stress-strain state in axisymmetric conditions, it is necessary to consider all the directions for example in the axisymmetric strain space (i.e. Rendulic Plane). For that it is introduced axisymmetric proportional strain loading paths defined incrementally by :

$$\begin{cases} d\varepsilon_1 & = & \text{positive constant} \\ d\varepsilon_2 & = & d\varepsilon_3 \text{ (axisymmetric condition)} \\ d\varepsilon_1 + 2Rd\varepsilon_3 & = & 0 \text{ (R constant for a given path)} \end{cases}$$

$R = 1$ corresponds to the undrained path which is characterized by the isochoric condition (no volume variation).
For $0 < R < 1$, the imposed path is dilatant, while for $1 < R$ it is contractant.
For this class of paths, the proper conjugate variables are $(\sigma_1 - \sigma_3/R)$ versus ε_1 and $(\varepsilon_1 + 2R\varepsilon_3)$ versus (σ_3/R) since : $\sigma_1\varepsilon_1 + 2\sigma_3\varepsilon_3 \equiv (\sigma_1 - \sigma_3/R)\varepsilon_1 + \sigma_3(\varepsilon_1 + 2R\varepsilon_3)/R$.
We have verified (Darve F. & Laouafa F. , 2001) numerically that, for a range of small R values, curve $(\sigma_1 - \sigma_3/R)$ versus ε_1 is passing through a maximum. This range of R values depends, of course, on the initial density of the sand (R must be smaller for a higher density). These curves can be considered as generalizations of $q - \varepsilon_1$ diagrams for undrained triaxial paths.
It is easy to verify that, at $(\sigma_1 - \sigma_3/R)$ peak, Lyapunov's definition is verified.
As regards Hill's condition, the second order work is equal to :

$$d^2W = (d\sigma_1 - d\sigma_3/R)d\varepsilon_1 + d\sigma_3(d\varepsilon_1 + 2Rd\varepsilon_3)/R \tag{2.11}$$

With the constraint : $d\varepsilon_1 + 2Rd\varepsilon_3 = 0$, it is clear that the second order work is vanishing at $(\sigma_1 - \sigma_3/R)$ peak and, after it, takes negative values. The constitutive equation can be written like that :

$$\begin{bmatrix} d\sigma_1 - d\sigma_3/R \\ d\varepsilon_1 + 2Rd\varepsilon_3 \end{bmatrix} = \begin{bmatrix} E_1^- & 2R\frac{E_1^-}{E_3^-}V_3^{1-} - 1 \\ 1 - 2RV_1^{3-} & \frac{2R^2\left(1-V_3^{3-}-2V_1^{3-}V_3^{1-}\right)}{E_3^-} \end{bmatrix} \begin{bmatrix} d\varepsilon_1 \\ d\sigma_3/R \end{bmatrix} \tag{2.12}$$

if we assume that $d\sigma_1$ and $d\sigma_3$ are negative (as given by the numerical results). At $(\sigma_1 - \sigma_3/R)$ peak, the bifurcation criterion is given by :

$$\det \underset{\sim}{S} = 0 \tag{2.13}$$

if $\underset{\sim}{S}$ is the constitutive matrix of relation (2.12). (2.13) gives the following equation in R :

$$2\frac{E_1^-}{E_3^-}\left(1 - V_3^{3-}\right)R^2 - 2\left(V_1^{3-} + \frac{E_1^-}{E_3^-}V_3^{1-}\right)R + 1 = 0 \tag{2.14}$$

which is an equation of second degree in R. It has two real solutions in R, if discriminant Δ is strictly positive :

$$\Delta = \left(V_1^{3-} + \frac{E_1^-}{E_3^-}V_3^{1-}\right)^2 - 2\frac{E_1^-}{E_3^-}\left(1 - V_3^{3-}\right) > 0 \tag{2.15}$$

or equivalently :

$$\Delta = -2\left(\frac{1 - V_3^{3-} - 2V_1^{3-}V_3^{1-}}{E_3^-}\right)^2 \det \underset{\sim}{Q}^S > 0$$

where $\underset{\sim}{Q}^S$ is the symmetric part of the constitutive matrix $\underset{\sim}{Q}$ given by :

$$\underset{\sim}{Q} = \begin{bmatrix} \frac{1}{E_1^-} & -\sqrt{2}\frac{V_3^{1-}}{E_3^-} \\ -\sqrt{2}\frac{V_1^{3-}}{E_1^-} & \frac{1-V_3^{3-}}{E_3^-} \end{bmatrix}$$

which relates $\begin{bmatrix} d\varepsilon_1 \\ \sqrt{2}d\varepsilon_3 \end{bmatrix}$ to $\begin{bmatrix} d\sigma_1 \\ \sqrt{2}d\sigma_3 \end{bmatrix}$ for $d\sigma_1 < 0$ and $d\sigma_3 < 0$ (see equation 2.10).
The unstable domain is thus characterized by : $\det \underset{\sim}{Q}^S < 0$ and its boundary by :

$$\det \underset{\sim}{Q}^S = 0 \tag{2.16}$$

Indeed, for incrementally linear constitutive relations,
$d^2W = \underset{\sim}{d\sigma}\,\underset{\sim}{d\varepsilon} = {}^t\underset{\sim}{d\sigma}\,\underset{\sim}{M}\,\underset{\sim}{d\sigma} \equiv {}^t\underset{\sim}{d\sigma}\,\underset{\sim}{M}^S\,\underset{\sim}{d\sigma}$, with : $\underset{\sim}{d\varepsilon} = \underset{\sim}{M}\,\underset{\sim}{d\sigma}$ and $\underset{\sim}{M}^S$ symmetric part of $\underset{\sim}{M}$.
In such a simple case, d^2W is vanishing only if $\det \underset{\sim}{Q}^S$ is vanishing (if the eigenvalues of $\underset{\sim}{M}^S$ are varying in a continuous manner from strictly positive initial values, what is always verified for realistic constitutive matrices).
For an incrementally piecewise linear relation (as considered here with the octo-linear model), we have 4 different constitutive matrices $\underset{\sim}{Q}$ following the signs of $d\sigma_1$ and $d\sigma_3$.
The discussion is thus more intricate, because the first unstable stress direction (which is given by the unique solution of equation (2.14) when discriminant Δ is vanishing) must belong to the tensorial zone defined by the signs of $d\sigma_1$ and $d\sigma_3$. Anyway the equation of the boundary of the unstable domain (if it exists) is given by :

$$\det \underset{\sim}{Q}^S = 0$$

where $\underset{\sim}{Q}^S$ is the symmetric part of constitutive matrix $\underset{\sim}{Q}$ associated to the proper tensorial zone.
At this boundary, the unique solution of (2.14) is equal to :

$$R_c = -\frac{\delta\varepsilon_1}{2\delta\varepsilon_3} = \frac{E_1^- V_3^{1-} + E_3^- V_1^{3-}}{2E_1^-\left(1 - V_3^{3-}\right)} \tag{2.17}$$

In Rendulic plane, the first unstable stress direction is then given by :

$$\frac{\delta\sigma_1}{\sqrt{2}\delta\sigma_3} = \frac{E_1^-\left(1 - V_3^{3-}\right)\left(E_1^- V_3^{1-} - E_3^- V_1^{3-}\right)}{\sqrt{2}E_3^-\left(E_1^-\left(1 - V_3^{3-} - V_1^{3-}V_3^{1-}\right) - E_3^-\left(V_1^{3-}\right)^2\right)} \tag{2.18}$$

with $\delta\sigma_1 < 0$ and $\delta\sigma_3 < 0$. These stress directions are plotted in figure 5.
The associated mode of rupture is characterized by the following rupture rule :

$$\underset{\sim}{S}\begin{bmatrix} d\varepsilon_1 \\ d\sigma_3/R \end{bmatrix} = \begin{bmatrix} 0 \\ 0 \end{bmatrix} \qquad \text{with} \qquad \det \underset{\sim}{S} = 0$$

where $\underset{\sim}{S}$ is the constitutive matrix defined by equation (2.12). It comes :

$$E_1^- d\varepsilon_1 + \left(2\frac{E_1^-}{E_3^-}V_3^{1-} - \frac{1}{R}\right) d\sigma_3 = 0 \tag{2.19}$$

At the bifurcation point (or equivalently at the limit stress-strain state) characterized by :

$$\begin{cases} d\sigma_1 - d\sigma_3/R &= 0 \\ d\varepsilon_1 + 2Rd\varepsilon_3 &= 0 \end{cases}$$

there are an infinite number of solutions (loss of uniqueness), but all these solutions must fulfilled constraint (2.19).
Note that these conclusions are perfectly similar to the plastic limit conditions discussed in the introduction (see general equations (1.3)and (1.4)), where :

$$\begin{cases} d\sigma_1 &= 0 \\ d\sigma_3 &= 0 \end{cases}$$

defines the plastic limit stress state, $\det \underset{\sim}{N} = 0$ is the plasticity criterion, and : $V_3^{1+}d\varepsilon_1 + d\varepsilon_3 = 0$ is the flow rule.
What is remarkable in equation (2.19) is the fact that it is a mixed condition, even if essentially this is the generalization of the notion of flow rule.
All these results have been verified numerically with the octo-linear model and with the thoroughly incrementally non-linear relation (for a presentation of this relation see chapter 1 by Darve and Servant and Darve F. et al. (1995)).
The strain proportional loading paths have been simulated for various values of R. Some maxima for $(\sigma_1 - \sigma_3/R)$ have been found for a certain range of R values (see figure 2).
Finally the cones of unstable stress directions have been plotted for a dense sand (figure 3) and a loose sand (figure 4). Note that for high stress levels there are two cones of unstable stress directions. Indeed the previous analytical results have just shown that there are possibly two solutions in R (what means one cone) inside one tensorial zone. Thus several cones can exist, when there are several tensorial zones.
In the next section, the case of plain strain conditions is considered.

2.3 Plane strain conditions

For plane strain conditions ($\varepsilon_2 = 0$) and coinciding stress-strain principal axes, the same reasoning can be developed.
The octo-linear constitutive model takes the following form :

$$\begin{bmatrix} d\varepsilon_1 \\ d\varepsilon_3 \end{bmatrix} = \begin{bmatrix} \frac{1-V_1^{2\pm}V_2^{1\pm}}{E_1^{\pm}} & -\frac{V_3^{1\pm}+V_3^{2\pm}V_2^{1\pm}}{E_3^{\pm}} \\ -\frac{V_1^{3\pm}+V_1^{2\pm}V_2^{3\pm}}{E_1^{\pm}} & \frac{1-V_2^{3\pm}V_3^{2\pm}}{E_3^{\pm}} \end{bmatrix} \begin{bmatrix} d\sigma_1 \\ d\sigma_3 \end{bmatrix} \tag{2.20}$$

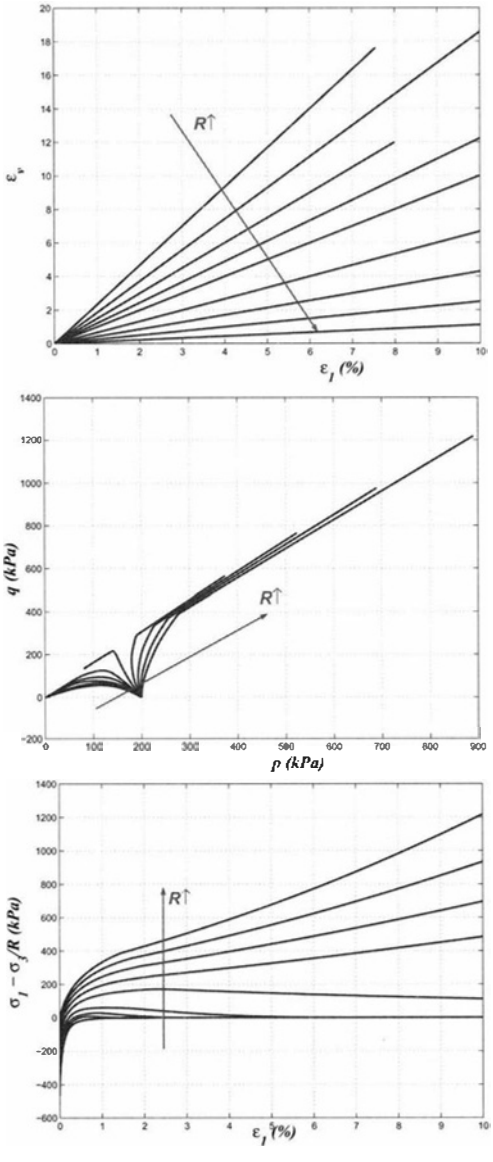

Figure 2. Proportional strain paths simulated by the incrementally non-linear model in the case of Hostun dense sand. $(\sigma_1 - \frac{\sigma_3}{R})$ possesses a maximum for low R values, $R \in \{0.3, 0.35, 0.4, 0.45, 0.5, 0.6, 0.7, 0.8, 0.9, 1.0\}$.

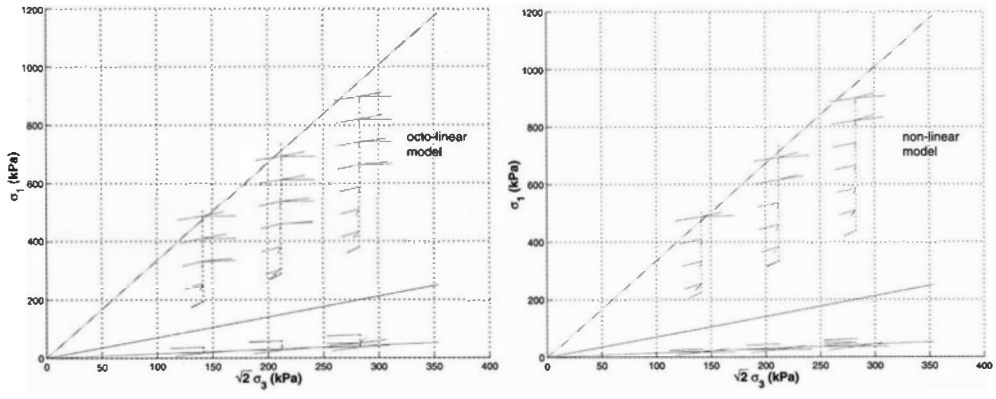

Figure 3. Cones of unstable stress directions and boundary of the unstable domain in Rendulic plane for dense Hostun sand in the cases of the octo-linear model (on the left) and of the non-linear one (on the right).

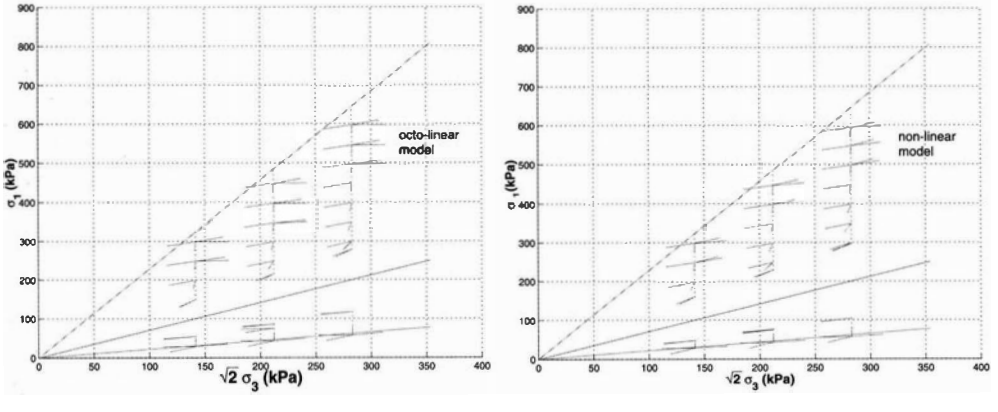

Figure 4. Cones of unstable stress directions and boundary of the unstable domain in Rendulic plane for loose Hostun sand in the cases of the octo-linear model (on the left) and of the non-linear one (on the right).

Following indices $(+,-)$, 2.20 corresponds to 8 different linear relations between $(d\varepsilon_1, d\varepsilon_3)$ and $(d\sigma_1, d\sigma_3)$ by taking into account the sign of $d\sigma_2$.
Let us consider proportional strain loading paths defined by :

$$\begin{cases} d\varepsilon_1 & = & \text{positive constant} \\ d\varepsilon_2 & = & 0 \\ d\varepsilon_1 + R d\varepsilon_3 & = & 0 \,(R \text{ constant for a given path}) \end{cases}$$

The conjugate variables are $(\sigma_1 - \frac{\sigma_3}{R})$ versus ε_1 and $(\varepsilon_1 + R\varepsilon_3)$ versus $(\frac{\sigma_3}{R})$.
The second order work is equal to :

$$d^2W = (d\sigma_1 - d\sigma_3/R)d\varepsilon_1 + d\sigma_3(d\varepsilon_1 + R d\varepsilon_3)/R \tag{2.21}$$

and will vanish at $(\sigma_1 - \frac{\sigma_3}{R})$ peak. If the tensorial zone $d\sigma_1 < 0, d\sigma_2 < 0, d\sigma_3 < 0$ is considered (this assumption has to be verified a posteriori), the octo-linear model can be written under the following form :

$$\begin{bmatrix} d\sigma_1 - d\sigma_3/R \\ d\varepsilon_1 + R d\varepsilon_3 \end{bmatrix} = \begin{bmatrix} \frac{E_1^-}{1-V_1^{2-}V_1^{1-}} & \frac{E_1^-(V_3^{1-}+V_3^{2-}V_2^{1-})}{E_3^-(1-V_1^{2-}V_2^{1-})}R - 1 \\ 1 - \frac{V_1^{3-}+V_1^{2-}V_2^{3-}}{1-V_1^{2-}V_2^{1-}}R & \frac{dR^2}{E_3^-(1-V_1^{2-}V_2^{1-})} \end{bmatrix} \begin{bmatrix} d\varepsilon_1 \\ \frac{d\sigma_3}{R} \end{bmatrix} \tag{2.22}$$

with $d = 1 - V_1^{2-}V_2^{1-} - V_1^{3-}V_3^{1-} - V_2^{3-}V_3^{2-} - V_1^{2-}V_2^{3-}V_3^{1-} - V_2^{1-}V_1^{3-}V_3^{2-}$.
Taking into account the loading constraint $d\varepsilon_1 + R d\varepsilon_3 = 0$, and, at $(\sigma_1 - \frac{\sigma_3}{R})$ peak, it comes the bifurcation criterion given by the vanishing determinant of constitutive matrix of relation 2.22 :

$$\begin{aligned} E_1^-(1 - V_2^{3-}V_3^{2-})R^2 - [E_3^-(V_1^{3-} + V_1^{2-}V_2^{3-}) + E_1^-(V_3^{1-} + V_3^{2-}V_2^{1-})]R \\ + E_3^-(1 - V_1^{2-}V_2^{1-}) = 0 \end{aligned} \tag{2.23}$$

As for axisymetric conditions an equation of second degree in R is found, which implies the existence of cones of unstable directions in a given tensorial zone (if the unstable directions belong to the tensorial zone which has been assumed a priori), when the discriminant is positive.
This discriminant is equal to :

$$\begin{aligned} \Delta = (E_3^-)^2(V_1^{3-} + V_1^{2-}V_2^{3-})^2 + (E_1^-)^2(V_3^{1-} + V_3^{2-}V_2^{1-})^2 \\ -2E_1^-E_3^-[d + (1 - V_2^{3-}V_3^{2-})(1 - V_1^{2-}V_2^{1-})] \end{aligned} \tag{2.24}$$

which can be put under the following form :

$$\Delta = -4(E_1^-)^2(E_3^-)^2 det \underset{\sim}{P}^S \tag{2.25}$$

where $\underset{\sim}{P}^S$ is the symmetric part of the constitutive matrix of relation 2.20 (with indices "-").
Once more, the boundary of the unstable domain is given by :

$$det \underset{\sim}{P}^S = 0 \tag{2.26}$$

(if the unstable directions correspond to $d\sigma_1 < 0$ and $d\sigma_3 < 0$)
The first unstable direction corresponds to :

$$R_c = -(\frac{d\varepsilon_1}{d\varepsilon_3})_c = \frac{E_3^-(V_1^{3-} + V_1^{2-}V_2^{3-}) + E_1^-(V_3^{1-} + V_3^{2-}V_2^{1-})}{2E_1^-(1 - V_2^{3-}V_3^{2-})} \tag{2.27}$$

or

$$(\frac{d\sigma_1}{d\sigma_3})_c = \frac{E_1^-(1 - V_2^{3-}V_3^{2-})[E_1^-(V_3^{1-} + V_3^{2-}V_2^{1-}) - E_3^-(V_1^{3-} + V_1^{2-}V_2^{3-})]}{E_3^-[E_1^-(d + (1 - V_1^{2-}V_2^{1-})(1 - V_2^{3-}V_3^{2-})) - E_3^-(V_1^{3-} + V_1^{2-}V_2^{3-})^2]} \tag{2.28}$$

Figures 5, 6 and 7 present the "first" unstable stress states (according to the level of stress deviator) respectively for the axisymmetric conditions (figure 5), for plane strain conditions (figure 6) and for 3D conditions in a deviatoric stress plane (figure 7). The stress curve or surface, which is obtained by linking these stress states, corresponds to the boundary of the "unstable" domain. Inside this stress unstable domain one can find various kinds of bifurcations and losses of uniqueness, which means various failure modes by material instabilities (localized failure, diffuse failure...) and geometric instabilities. These failure modes depend on the previous stress-strain history, on the current incremental stress direction and on the loading mode (stress controlled, strain controlled...).

Hill's condition of stability is essentially a directional quantity (see equation 2.8) since

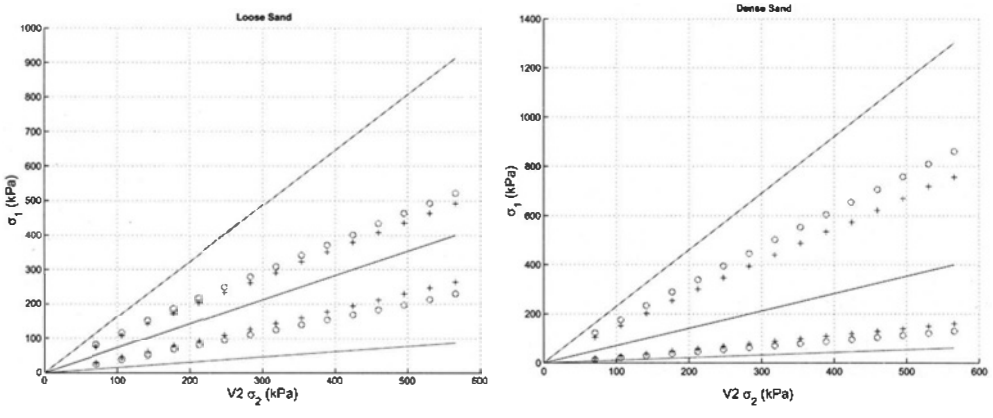

Figure 5. Domains of instability in Rendulic Plane and axisymmetric conditions for the loose sand on the left, for the dense sand on the right and for 2 different constitutive relations (symbols "o" and "+" for the incrementally non-linear and the octolinear models respectively).

:

$$\frac{d^2W}{\|d\underset{\sim}{\sigma}\|^2} = {}^t\underset{\sim}{u}\underset{\sim}{M}(\underset{\sim}{u})\underset{\sim}{u} \tag{2.29}$$

It follows that there are cones of unstable stress directions, as plotted in figures 3 and 4. The first unstable direction is progressively opening into a cone when the stress deviator

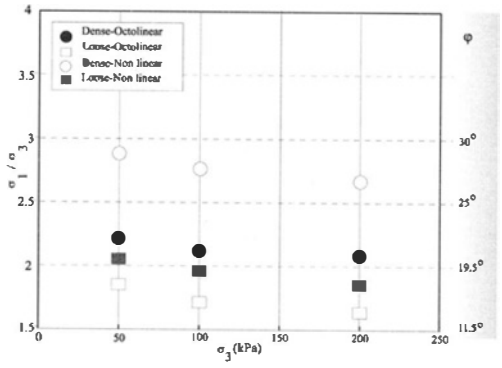

Figure 6. Lowest unstable stress levels in plane strain conditions for the loose and dense sand, for 2 different constitutive relations.

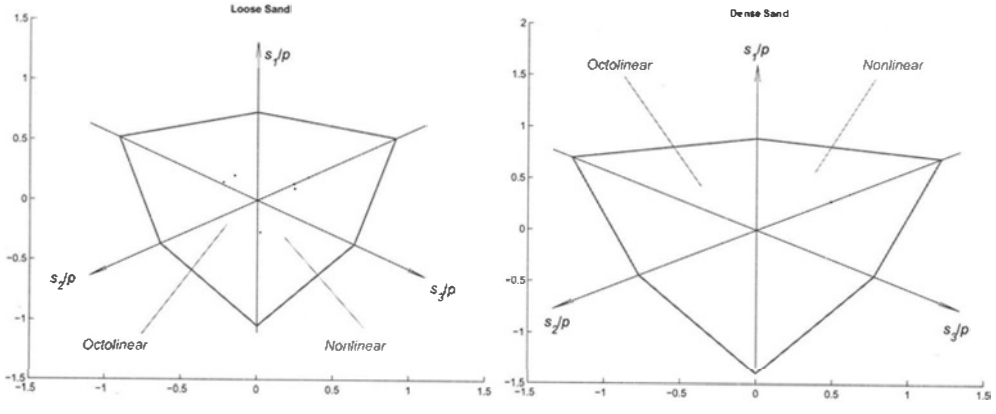

Figure 7. Domain of instability in deviatoric plane for the loose and dense sand, and for 2 different constitutive relations.

is increasing. The limit directions of these cones are given by th solutions of equation 2.14 for axisymetric conditions and the solutions of 2.23 in plane strain conditions. It is worth to note in figures 3 and 4 that the vertical stress direction (which corresponds to drained triaxial tests) is never inside the cones. Along drained triaxial compressions or extensions it is impossible to obtain diffuse failure, which is a well known experimental fact.

3 q-constant loading paths : an example

3.1 Analysis

At a given stress-strain state, q-constant axisymmetric loading paths consist in maintaining q constant by an incrementally isotropic unloading defined by : $d\sigma_1 = d\sigma_2 =$

$d\sigma_3$ = negative constant.
The proper conjugate variables to analyse this path are : $\varepsilon_v - \sigma_3$ and $q - \varepsilon_1$, where : $\varepsilon_v = \varepsilon_1 + 2\varepsilon_3$, because we have :

$$W = \sigma_1\varepsilon_1 + 2\sigma_3\varepsilon_3 = \varepsilon_v\sigma_3 + q\varepsilon_1 \tag{3.1}$$

The second order work can thus be written as follows : $d^2W = d\varepsilon_v d\sigma_3 + dq d\varepsilon_1$, and with the constraint : $dq = 0$, it comes :

$$d^2W = d\varepsilon_v d\sigma_3 \tag{3.2}$$

If ε_v passes through a minimum value, this minimum will be an unstable state according to Hill's condition. On the contrary σ_3 is monotonously decreasing.
As the relative volume variations $\frac{\Delta V}{V_0}$ is equal to $(-\varepsilon_v)$: $\frac{\Delta V}{V_0} = -\varepsilon_v$, the minimum for ε_v is a maximum for $\frac{\Delta V}{V_0}$.
Thus a "small" additional positive volume variation (for a volume variation controlled loading) induces a sudden failure of the sample. It can be concluded that this maximum of volume variations is unstable following Lyapunov's definition of stability.
Now if the constitutive relation is written under the following form (for axisymmetric conditions) :

$$\begin{bmatrix} d\varepsilon_v \\ dq \end{bmatrix} = \underset{\sim}{T} \begin{bmatrix} d\sigma_3 \\ d\varepsilon_1 \end{bmatrix} \tag{3.3}$$

the analysis can be carried out as previously.
Along the path the constraint : $dq = 0$ is fulfilled and, at ε_v minimum, $d\varepsilon_v$ is zero.
Thus, the bifurcation criterion is given by :

$$\det \underset{\sim}{T} = 0 \tag{3.4}$$

and the rupture rule by :

$$\underset{\sim}{T} \begin{bmatrix} d\sigma_3 \\ d\varepsilon_1 \end{bmatrix} = \begin{bmatrix} 0 \\ 0 \end{bmatrix} \tag{3.5}$$

Note that equations (3.4) and (3.5) are exactly equivalent to equations (2.6), what means that bifurcation criterion and rupture rule are the same for q-constant loading path and for undrained loading. Thus the results of the subsection 2.2 apply with constant R equal to 1.
With our octo-linear model, the bifurcation criterion is given by :

$$2\frac{E_1^-}{E_3^-}\left(1 - V_3^{3-} - V_3^{1-}\right) + 1 - 2V_1^{3-} = 0 \tag{3.6}$$

The rupture rule corresponds to :

$$E_1^- d\varepsilon_1 + \left(2\frac{E_1^-}{E_3^-}V_3^{1-} - 1\right) d\sigma_3 = 0 \tag{3.7}$$

The unstable stress direction is obviously given by : $d\sigma_1 = d\sigma_3$ and it is parallel to the hydrostatic line.

Finally one question is remaining open : are the volume variations possessing a maximum for a certain range of initial densities and a certain range of stress levels ? To answer to this question in the next subsection, we have simulated q-constant loading paths with our constitutive relations.

3.2 Numerical modelling

q-constant paths have been simulated with our octo-linear model and with the non-linear one. Figures 8 and 9 present the results for loose Hostun sand and for initial isotropic pressures respectively equal to 100 kPa and 500 kPa. When the second order work is negative, the computed points are replaced by different symbols (triangles, squares, circles, depending on the value of q, see figure 8). The diagrams are composed of two parts. A first part is constituted by a triaxial compression until reaching various q values. Then q is maintained constant.

These results allow to validate our previous assumptions. For example, lateral pressure is decreasing monotonously. On the contrary the volume variations are indeed possessing a maximum. Of course it is verified that from this maximum, the second order work is negative.

Figure 10 shows the results obtained with dense Hostun sand. The same comments as previously are pertinent, except the fact that the volume variations do not reach any maximum. Note that the computations are stopped when Mohr-Coulomb plastic limit condition is reached. The second order work is always strictly positive.

These results could have been drawn from figures 3 and 4. q-constant loading paths are parallel to the hydrostatic axis. We see that this direction is included inside the cone of unstable directions for low q/p values for loose Hostun sand and not at all for any q/p value for the dense one.

Modelling has been also performed with the incrementally non-linear model with similar conclusions (see figure 11 for such a comparison).

Several conclusions can be drawn.

The most important one is certainly the fact that a diffuse mode of failure, which was repeatedly noted in experiments (Chu J. & Leong W.K., 2003), can be properly analyzed by Hill's condition of stability.

It has been also shown that the bifurcation criterion and the failure rule are the same for undrained (i.e. isochoric) paths and q-constant paths. Finally a generalization of the notion of limit state has been brought out. For q-constant paths the stresses are monotonously decreasing ($d\sigma_1 = d\sigma_2 = d\sigma_3 < 0$) while the dilatancy is reaching a maximum value. If one injects at this maximum a small amount of water inside the sample, a sudden failure is occurring without any localization pattern. Thus we can expect the existence of a limit surface in the strain space (dual of the classical limit surface in the stress space). Indeed the strains are limited on the hydrostatic axis or for one-dimensional compressions.

Next section is now devoted to investigate a possible application of Hill's condition in discrete mechanics.

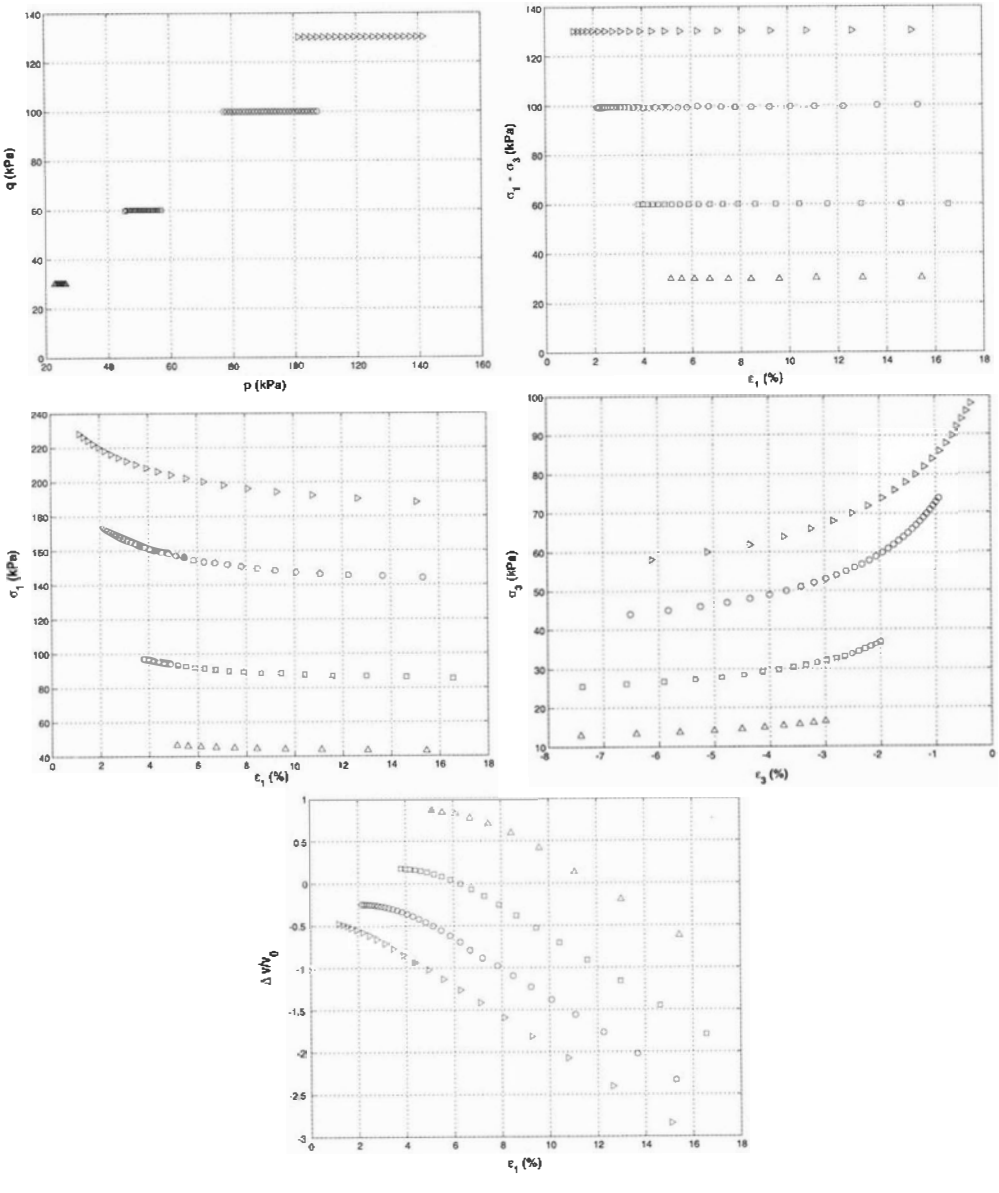

Figure 8. Simulation of q-constant loading paths for loose Hostun sand by the octolinear constitutive model. Points are replaced by other symbols when the second order work takes negative values from the maximum of volume variations. The initial isotropic pressure is equal to 100 kPa.

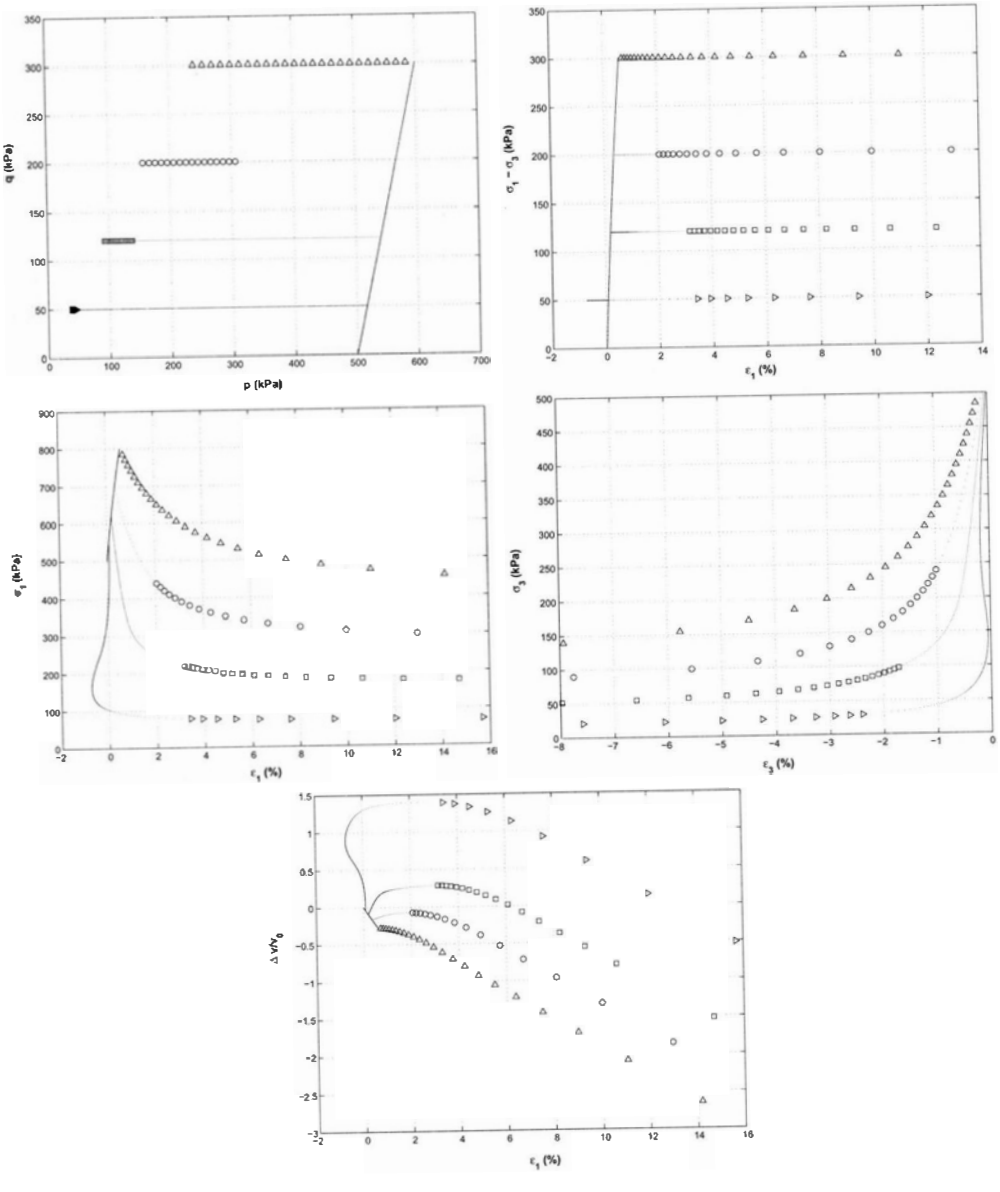

Figure 9. Simulation of q-constant loading paths for loose Hostun sand by the octolinear constitutive model. Points are replaced by other symbols when the second order work takes negative values from the maximum of volume variations. The initial isotropic pressure is equal to 500 kPa.

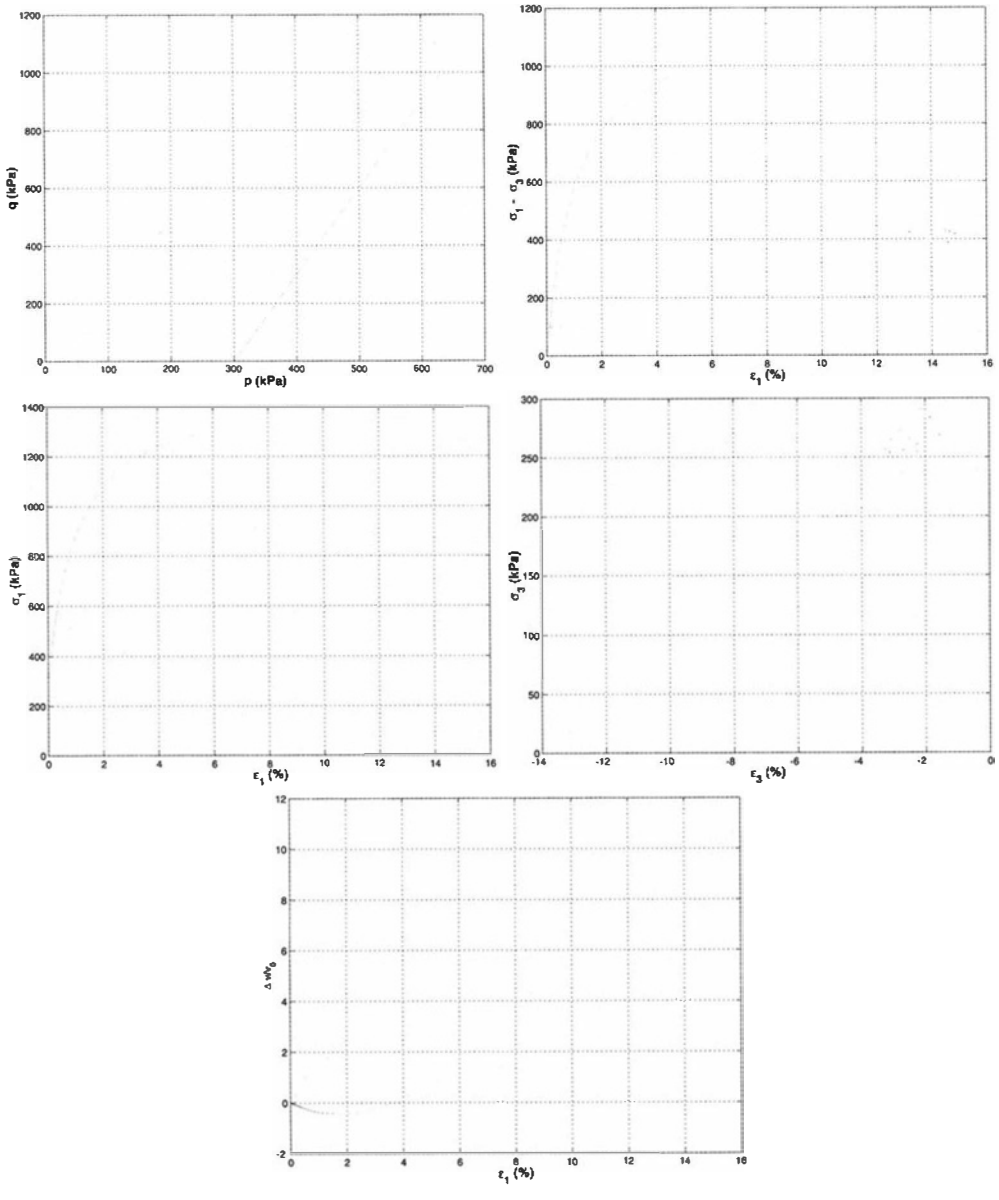

Figure 10. Simulation of q-constant loading paths for dense Hostun sand by the octolinear constitutive model. The second order work is never vanishing.

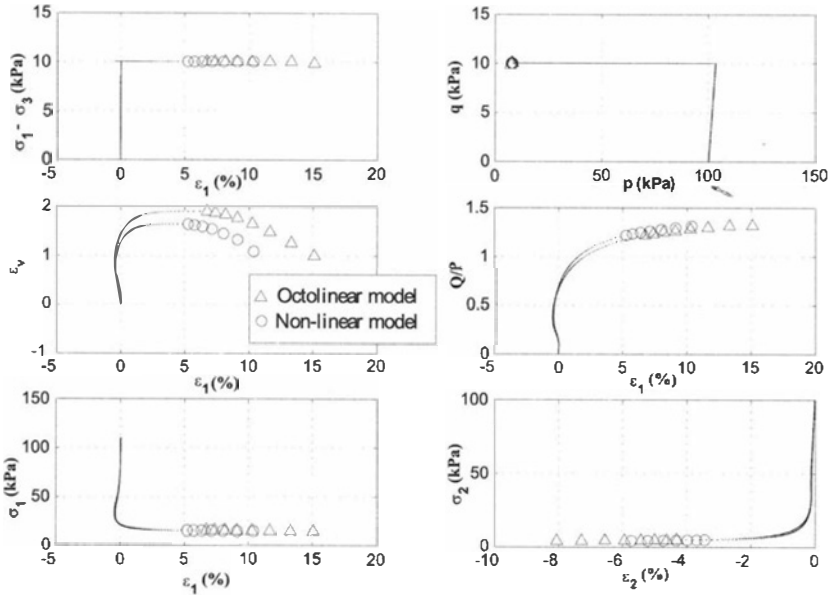

Figure 11. Simulation of q-constant loading paths for loose Hostun sand by the octolinear and the non-linear constitutive model. Points are replaced by other symbols when the second order work takes negative values from the maximum of volume variations. The initial isotropic pressure is equal to 100 kPa.

4 Grain avalanches

Granular media are characterized by a double nature : continuous and discrete.
For some phenomena (experiments on homogeneous samples, in situ behavior at large scale,...) they behave like continuous media , the assumption of matter continuity represents a proper description, stresses, strains and constitutive relations are pertinent tools and the framework of continuum mechanics is adequate.
For other phenomena (granular segregation, mixing of two granular populations,...) they behave like discrete media, each grain has to be considered as a specific individual, forces, displacements, rotations and local granular interactions are pertinent tools, while the framework of discrete mechanics is convenient. Grain avalanches along a slope are certainly a consequence of discrete nature of granular media. Thus, in this section, we have to introduce discrete notions, discrete tools and finally to perform discrete computations.

4.1 Discrete second order work and kinetic energy

In this section we consider only two-dimensional granular materials which are constituted by piled cylinders (the so-called Schneebeli material). All the variables are thus defined in a two-dimensional space.
A given grain is subjected to several forces due to the other grains in contact and due to gravity. The resultant force is called $\overrightarrow{F}$. Under the force increment $\overrightarrow{dF}$ the grain is moving of $\overrightarrow{dl}$. All these forces are also developing torques along the cylinder axes. The resultant torque is noted C, whose consequence is a rotation Ω around the axis.
Thus the discrete second order work is defined by (Mandel J. , 1966) :

$$d^2W = \overrightarrow{dF}.\overrightarrow{dl} + dCd\Omega \tag{4.1}$$

The objective is to investigate a possible link between discrete second order work and failure in discrete media, as an extension of the previous results which have shown such a link between second order work and diffuse failure.
In discrete media, failure at free surface is generally characterized by granular avalanches. During these avalanches the kinetic energy is varying a lot from zero values to maxima, then again to zero values. Thus kinetic energy has been chosen as a proper variable to characterize a grain avalanche from a mechanical point of view.
For a given grain its expression is :

$$e_c = \frac{1}{2}mv^2 + \frac{1}{2}I\omega^2 \tag{4.2}$$

where m is the grain mass, v its speed, I the inertia moment around the cylinder axis and ω the rotation speed.
Second order work and kinetic energy have been defined for a given grain. It is also interesting to consider their values for the whole assembly of grains as follows :

$$\begin{cases} D^2W &= \sum_{k=1}^{N} d^2W_k \\ E_c &= \sum_{k=1}^{N} e_c^k \end{cases} \tag{4.3}$$

where N is the total number of grains.

4.2 Discrete material and discrete numerical method

The granular medium is a two-dimensional material constituted by wood piled cylinders. The diameters are equal to 13, 18 and 28 mm. There are around 350 particles for a given experiment simulated by a discrete numerical method. The large dimensions of the grains allow an automatic image acquisition and data processing. From this photographic technique it is possible to extract incremental displacement and rotation fields (or the corresponding velocity fields) for the whole granular assembly.
The experiments have been performed in a plane shear box (Joer H. et al. , 1992) which allows to apply loading programs at the boundary of the slope. In this paper two cases are presented in a more detailed manner, even if the conclusions are also valid for the other cases not considered here. The first case is constituted by an active failure of the

slope by pulling the retaining vertical wall outside of the granular assembly (see figure 12(a)), the second case is a slope "loaded at his top", where avalanches are induced by a vertical loading on the flat top of the slope (see figure 12(b)). The configurations of the grain assemblies, as they are appearing on figure 12, are the real experimental ones. These initial configurations are exactly reproduced numerically in order to have a realistic granular assembly. Indeed the numerical experiments have shown the great influence of the initial configuration on the following deformations and failures. With this procedure (i.e. the simulation of experimental initial configurations), a good agreement has been found between the experimental displacement/rotation fields and the numerical ones (Darve F. et al. , 2003). This question is not discussed here, where it is chosen to focus on the mechanical analysis of the numerical results. The numerical discrete

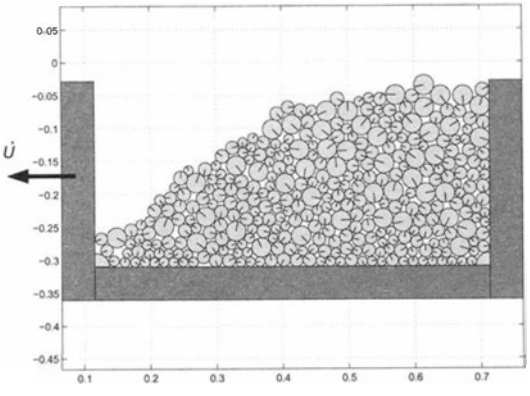

(a)

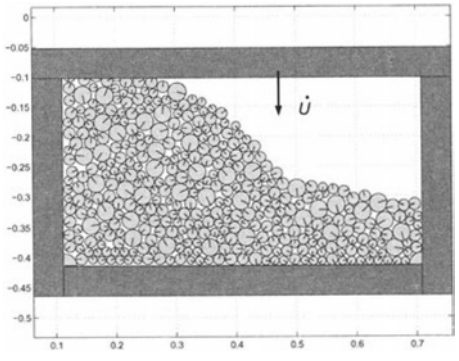

(b)

Figure 12. Configurations of the slope and loading programmes to induce granular avalanches in a two-dimensional medium.

method which has been utilized is based on the "Contact Dynamics" theory as developed by Moreau J.J. (1994). The numerical code has been achieved by Lanier J. & Jean M.

(1994).
This method is essentially different from the one proposed by Cundall P.A. & Strack O.D.L. (1979), because the numerical algorithm for time integration is implicit and also because the interactions between grains are not described by springs, slides and dashpots. In the Contact Dynamics method, the grains are assumed perfectly rigid. Thus there is a kinematic constraint constituted by the non-penetrability condition (the so-called Signorini condition, see figure 13(a)). The granular interactions are described by a simple coulombian friction, as represented on figure 13(b). If μ is the friction coefficient between grains, a tangential displacement U_t is allowed only if the tangential component R_t of the interaction force is equal to : $\pm\mu R_n$, where R_n is the normal component (figure 13(b)). For these simulations the friction coefficient between grains has been estimated to 0.5317 and between grains and walls to 0.25. Note that both these coefficients are the only mechanical parameters introduced in the computation. The other data have a geometric nature and are constituted by the initial configuration of the grain assembly, as discussed before.

Figure 13. Illustrations of the non-penetrability condition 13(a) and of the coulombian friction 13(b), where R_n and R_t are respectively the normal and tangential components of the interaction force and μ the friction coefficient. δ is the "distance" (roughly) between two grains and U_t the tangential inter-granular displacement.

4.3 Grain avalanches by active failure of the slope

In this case the number of grains is equal to : $N = 335$, the displacement speed (see figure 12(a)) to 10^{-2} m/s (the physical time has however not any influence on the computation). There are 1080 increments of computation (the time increment is : 5.610^{-3}s).

Figure 14 presents a comparison between the measured displacement fields (on the left) and the computed values (on the right) for 4 values of the plate displacement. A first conclusion is obvious : the utilized discrete element method is able to capture the main characteristics of the successive grain avalanches thanks to the taking into account of the initial configuration of the grain assembly in the experiments. A second aspect is the fact that various failure modes are visible on figure 14. Some modes are deep and seem to be localized because of parallel displacement vectors (as for rigid body motions), while others are surficial and correspond to classical grain avalanches. These different failure modes (local or more global) will be characterized later on by bursts of kinetic

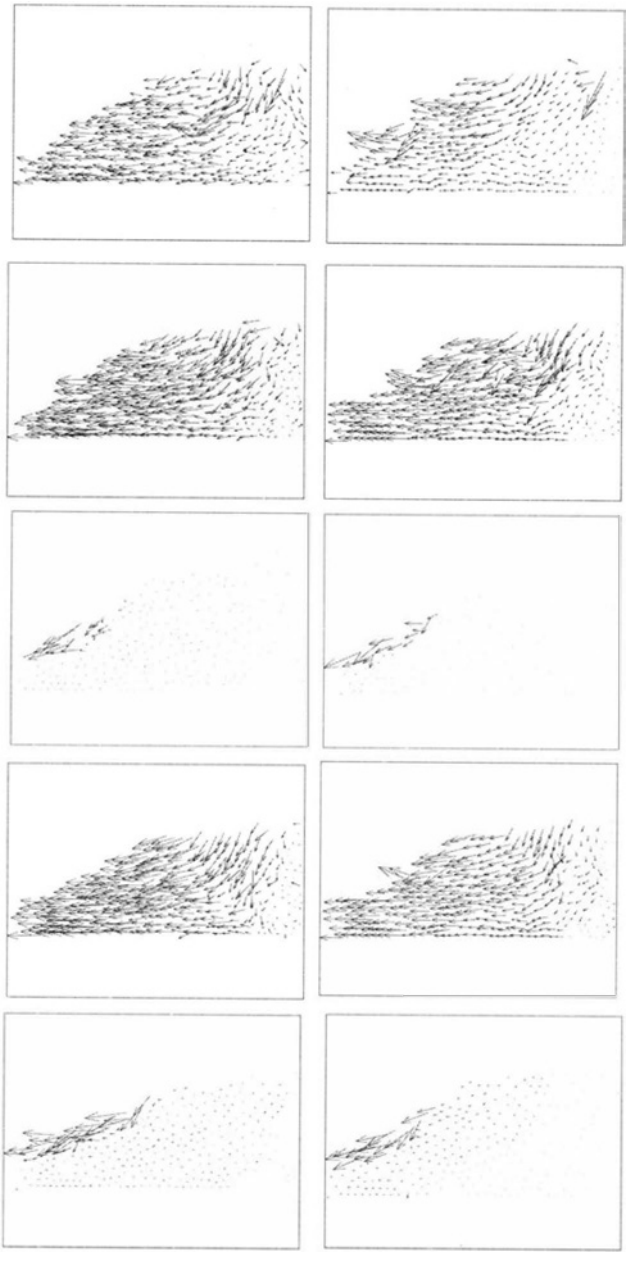

Figure 14. Experimental (on the left) and numerical (on the right) displacements fields for various plate displacements (see figure 12(a))

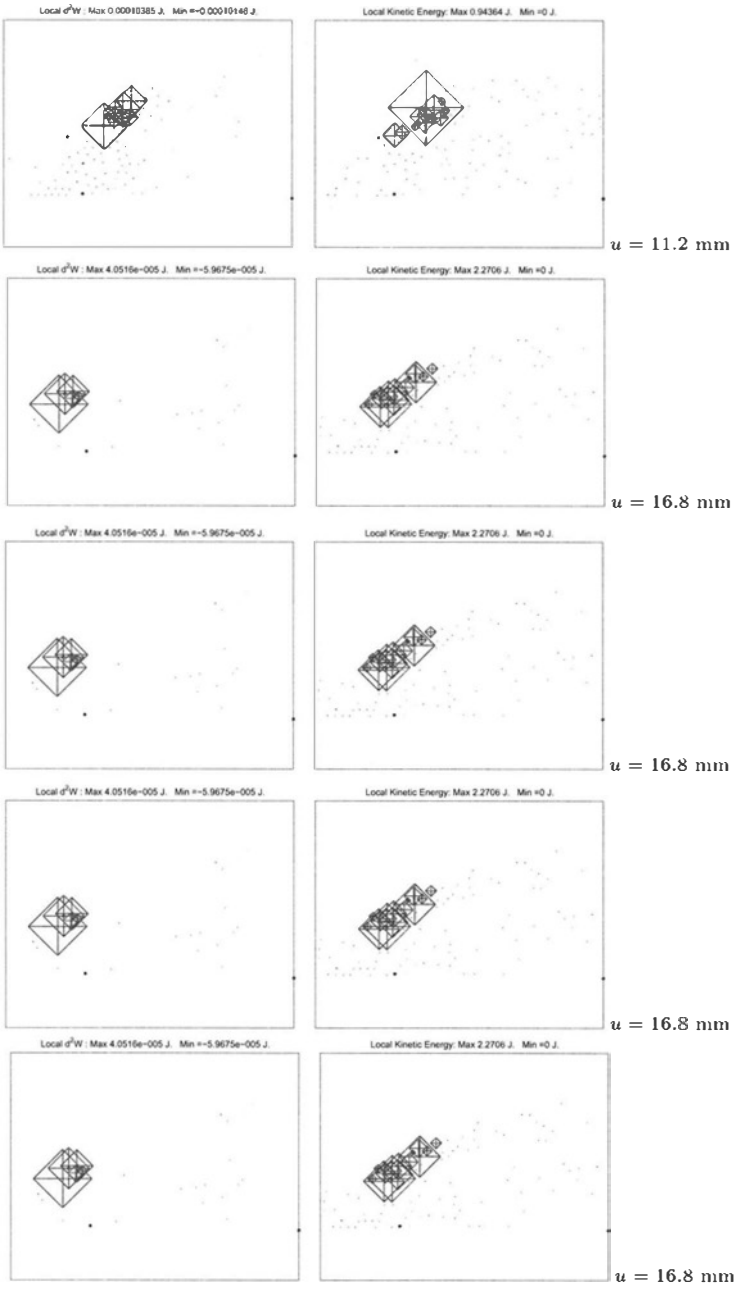

Figure 15. Spatial comparison between negative values of second order work d^2W (on the left) and the values of kinetic energy e_c (on the right).

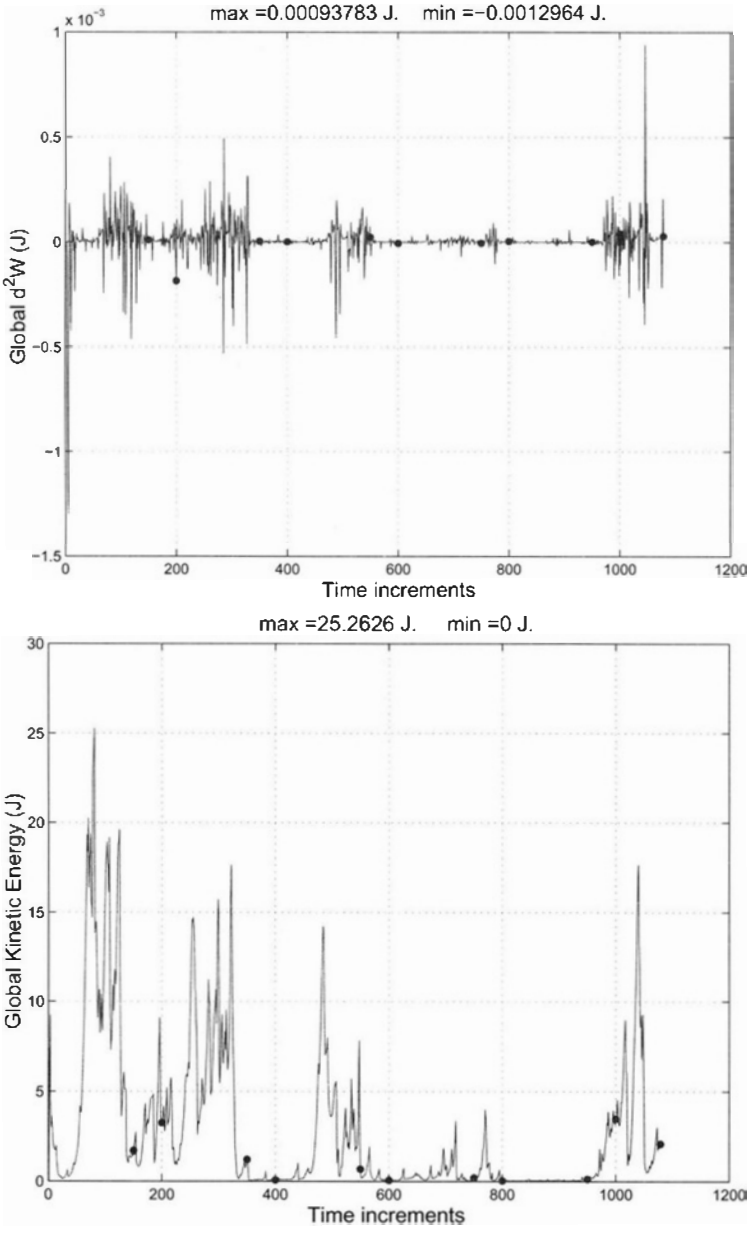

Figure 16. Comparison between global second order work and global kinetic energy as functions of plate displacement (equivalently number of time increments).

energy of various amplitudes.
Figure 15 shows a spatial comparison between the negative values of discrete second order work and the kinetic energy of the grains. The dimensions of the square symbols are proportional to the intensity of the scalar variables d^2W and e_c. The main failure mode is surficial with erratic fields of kinetic energy confirming the essential features of grain avalanches. However the most important point to be noticed is the spatial correlation between both the area where grains have negative second order work and where grains have bursts of kinetic energy. It is worthy to note also that the correlation is not attached to grains (a grain with or without negative second order work may or not move) but to area which can be characterized as "unstable".
This correlation is also a temporal one. Let us consider now the global quantities D^2W and E_c determined by adding the local values of each grain. Figure 16 presents such a comparison. Each point on both graphs corresponds to one computation, which means that there are exactly 1080 points.
All the values of D^2W have been plotted : the positive as the negative ones. Some conclusions are obvious from these results like the fact that the global second order work is varying suddenly from positive values to negative ones. Moreover, large positive values are associated to strong negative ones (the diagram is more or less symmetric with respect to the axis $D^2W = 0$). Indeed, the second order work is linked to energy, which can not be extracted in a finite manner from the medium. As regards the global kinetic energy variations, figure 16 shows successive 5 large failures for numbers of increments equal to 0, 90, 310, 490 and 1040. Smaller events (i.e. more surficial grain avalanches) occur for increment numbers of 200, 520, 710 and 760. Now let us go to the global second order work variations on same figure. We find 5 large minima for the negative values of D^2W and also 4 smaller relative minima for respectively the same 9 increment numbers. For example the small grain avalanches at increment 710 and 760 are clearly noticeable on D^2W graph by relative minima. This strong correlation is the manifestation of the deep link between failure and second order work.
Another example is presented in the next sub section.

4.4 Grain avalanches by loading at the top

Here the number of grains is equal to : $N = 377$. The vertical displacement rate of the plate is : 10^{-3} m/s (see figure 12(b)). The loading programme is still divided into 1000 increments. The friction coefficients are the same as before.
Figure 17 shows the incremental displacements fields for 8 values of the vertical displacement of the plate. Two different failure modes appear here. For plate displacements equal to 2.1, 25.2, 51.1 mm it seems that there is a deep localized failure mechanism exhibiting a rotation of a rather solid body. On the contrary, for plate displacements equal to 5.6, 23.1, 31.5, 35 mm the failure mechanism is rather a grain avalanche with a chaotic displacement field for the involved grains. From this rough analysis it appears difficult to conclude for the last case (plate displacement equal to 57.4 mm).
On figure 18 the spatial comparison between the area where the local second order work takes negative values and the one where the local kinetic energy is finite is presented. As before (see figure 15), a correlation between both areas seems to exist.

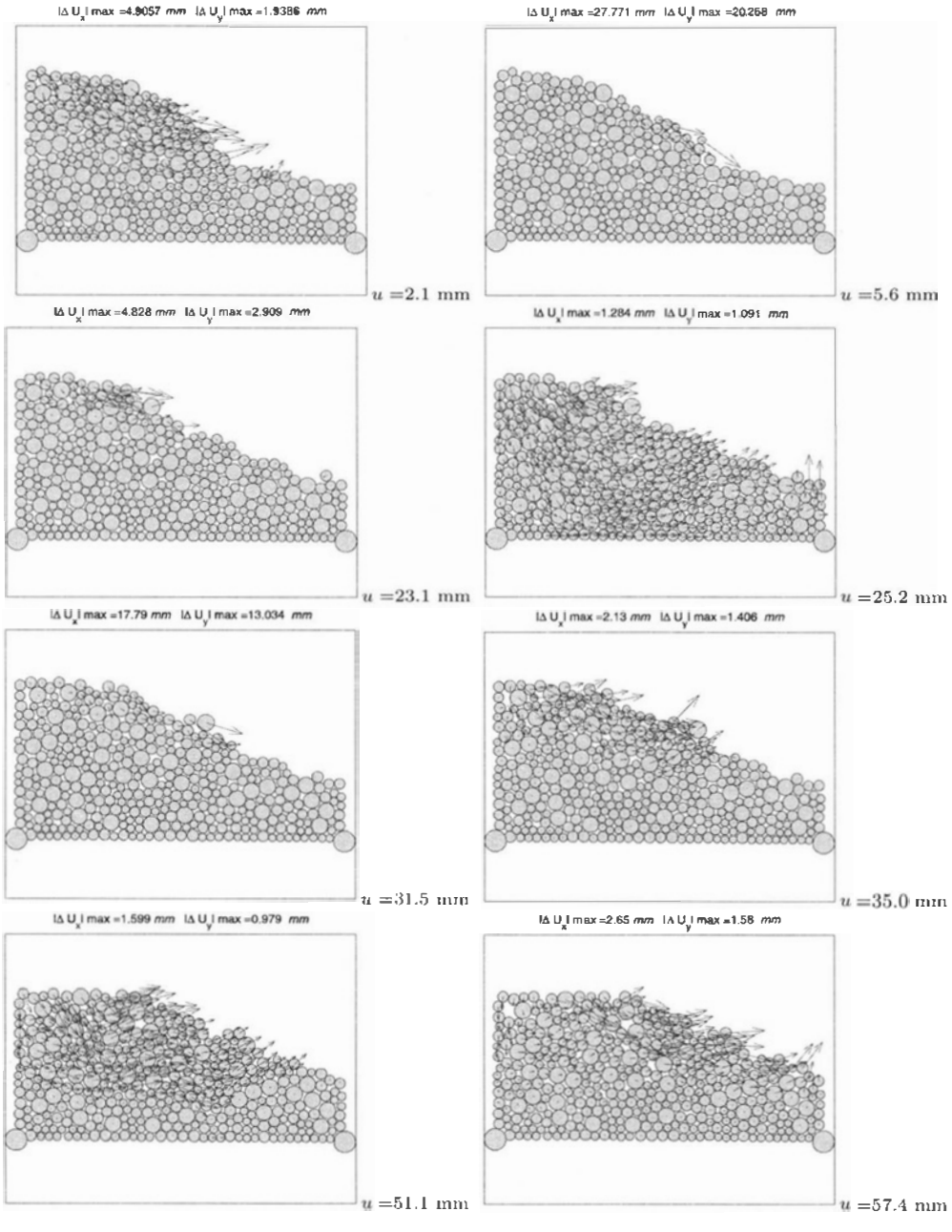

Figure 17. Field of incremental displacements at different values of vertical plate displacement u.

Figure 19 shows the temporal correlation between the bursts of global kinetic energy and the minima of negative values for the global second order work. From the kinetic energy variations there are 5 visible events for plate displacements of about 7, 14, 32, 46 and 65 mm. 5 events are also clearly distinguishable on the second order work diagram for 5, 14, 31, 46 and 65 mm.

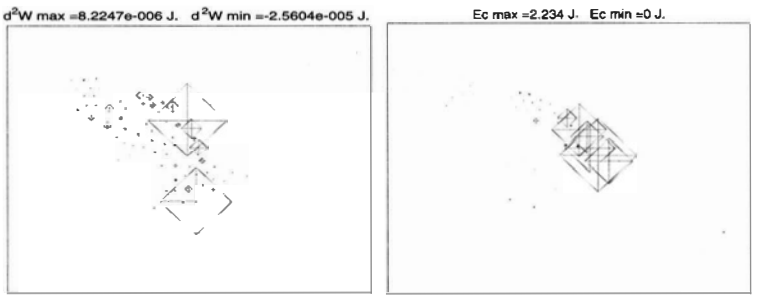

$u = 2.1$ mm

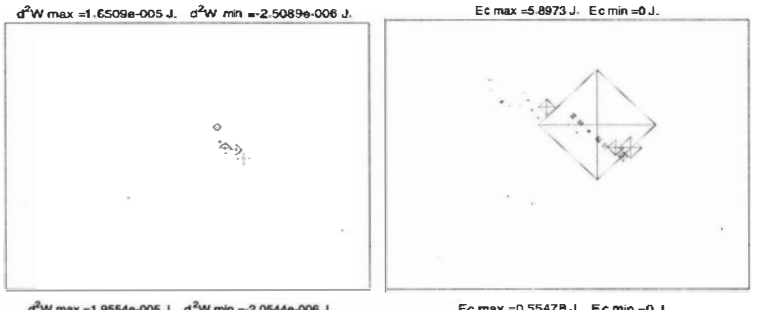

$u = 5.6$ mm

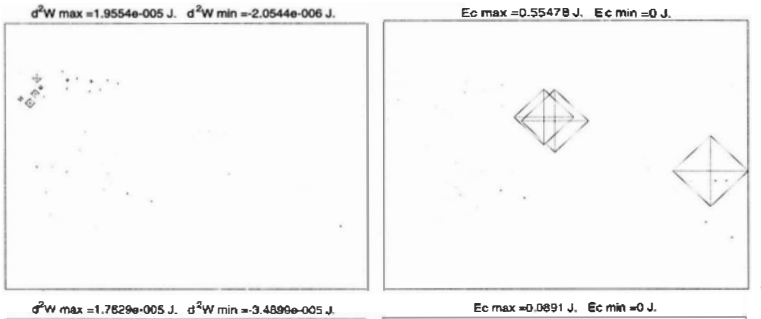

$u = 23.1$ mm

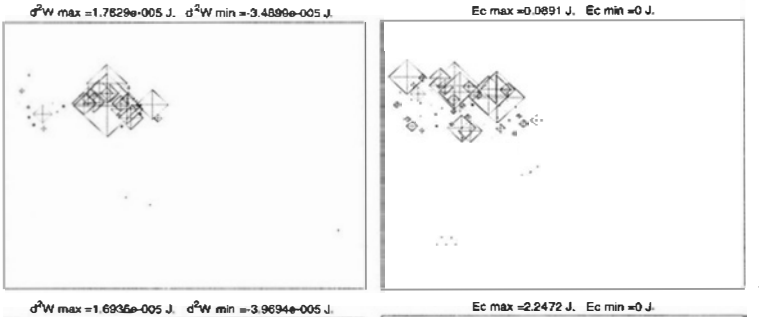

$u = 25.2$ mm

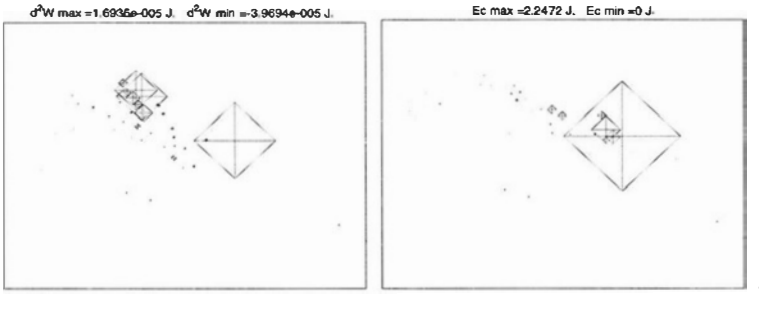

$u = 31.5$ mm

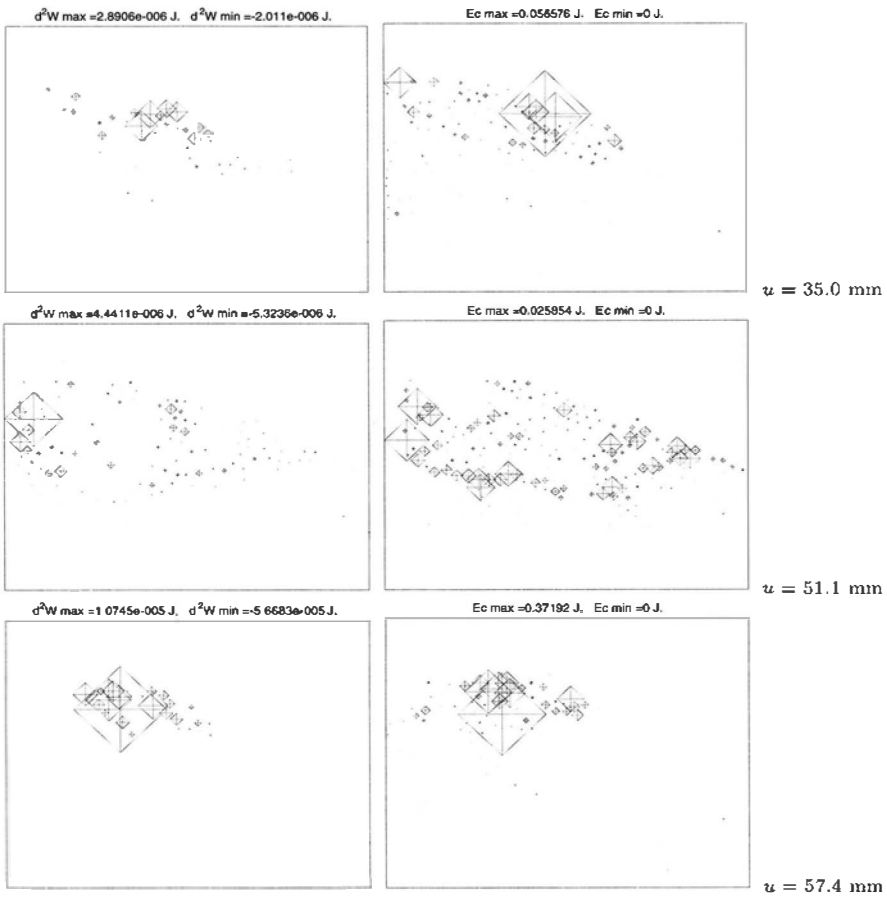

Figure 18. Spatial comparison between the negative values of second order work d^2W (on the left) and the values of kinetic energy e_c (on the right).

5 Conclusion

From an experimental point of view first, it has been shown that the question of failure in geomaterials has to be revisited. The peak of q in undrained conditions for a loose sand does satisfy neither the Mohr-Coulomb's plastic limit condition nor a strain localization criterion, but the failure is predicted by Hill's condition. Secondly this kind of failure states (located strictly inside the plastic limit surface and a localization condition) can be expected from the theory of non-associated hardening elasto-plasticity. Thirdly the numerical analysis carried out with an incrementally piece-wise linear and an incrementally non-linear constitutive relation have shown the existence of a whole stress domain where Hill's condition of stability is lost. In this domain, failure is characterized by bifurcation phenomena, losses of uniqueness and instabilities in Lyapunov's sense. Various modes

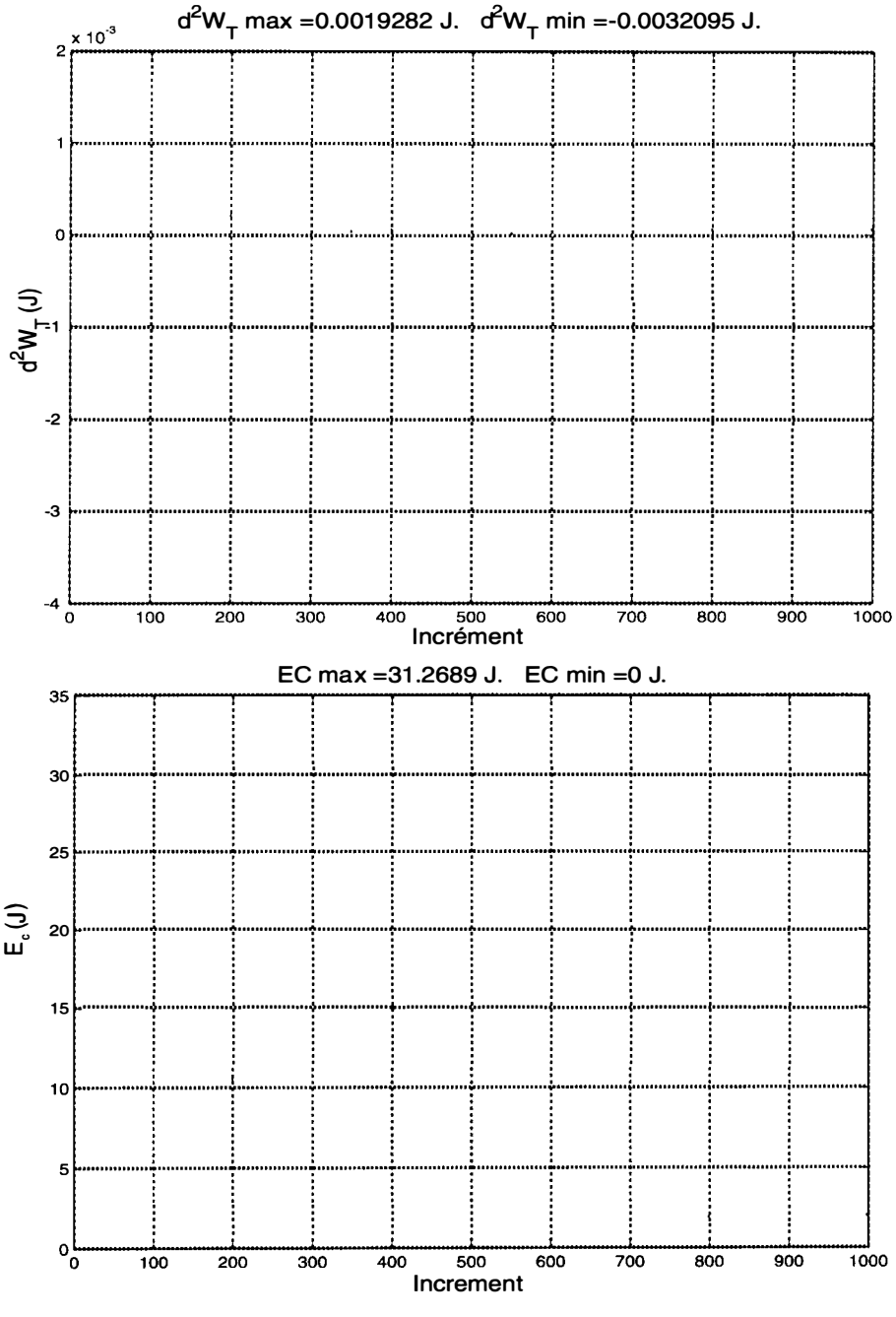

Figure 19. Comparison between global second order work and global kinetic energy as functions of the vertical plate displacement(or equivalently the number of time increments).

of failure can develop (localized, diffuse, due to geometric instabilities...). It seems that diffuse modes of failure can be analyzed by Hill's condition of stability.
The equation of the boundaries of the failure domain has been given and discussed, as the equations of the cones of unstable stress directions. Diffuse modes of failure can appear only if the stress state lies inside the failure domain, if the loading direction is included inside the cone of unstable directions and if proper loading modes (stress controlled) are considered. For boundary value problems (cases not considered in this paper), the global second order work (i.e. integrated on the whole body) and the symmetric part of the matrix of rigidity have to be analyzed.
The specific case of q-constant loading paths has been considered. It has been shown that the unexplained diffuse modes, exhibited in triaxial experiments on a loose sans along these paths, can be predicted by Hill's condition of stability.
In a second part, the phenomenon (of discrete nature) of grain avalanches has been tackled. The grain motions have been characterized by local and global kinetic energies. Surprisingly strong correlations between the bursts of kinetic energy and the negative values of second order work have been derived.
As a general conclusion, it appears that the sign of second order work (under both its continuous and its discrete forms) could constitute a proper criterion to detect certain modes of failure, which appear before the localized failure but for specific loading conditions given in the paper in the framework of continuum mechanics.
The application to natural hazards driven by gravity (landslides, debris flows, rockfalls, snow avalanches) is of great interest since some of them can not be explained in a classical plasticity framework.

Acknowledgements

The supports of European projects DIGA (5^{th} PCRD), LESSLOSS (6^{th} PCRD) and french national projects PIR (RGCU) and ACI CatNat (2002) are gratefully acknowledged.

Figure 1 Example of an unstable state related to a diffuse mode of failure strictly inside Mohr-Coulomb plastic limit condition : typical undrained triaxial behavior of a loose sand.

Figure 2 Proportional strain paths simulated by the incrementally non-linear model in the case of Hostun dense sand. $(\sigma_1 - \frac{\sigma_3}{R})$ possesses a maximum for low R values, $R \in \{0.3, 0.35, 0.4, 0.45, 0.5, 0.6, 0.7, 0.8, 0.9, 1.0\}$.

Figure 3 Cones of unstable stress directions and boundary of the unstable domain in Rendulic plane for dense Hostun sand in the cases of the octo-linear model (on the left) and of the non-linear one (on the right).

Figure 4 Cones of unstable stress directions and boundary of the unstable domain in Rendulic plane for loose Hostun sand in the cases of the octo-linear model (on the left) and of the non-linear one (on the right).

Figure 5 Domains of instability in Rendulic Plane and axisymmetric conditions for the loose sand on the left, for the dense sand on the right and for 2 different constitutive relations (symbols "o" and "+" for the incrementally non-linear and the octolinear models respectively).

Figure 6 Lowest unstable stress levels in plane strain conditions for the loose and dense sand, for 2 different constitutive relations.

Figure 7 Domain of instability in deviatoric plane for the loose and dense sand, and for 2 different constitutive relations.

Figure 8 Simulation of q-constant loading paths for loose Hostun sand by the octo-linear constitutive model. Points are replaced by other symbols when the second order work takes negative values from the maximum of volume variations. The initial isotropic pressure is equal to 100 kPa.

Figure 9 Simulation of q-constant loading paths for loose Hostun sand by the octo-linear constitutive model. Points are replaced by other symbols when the second order work takes negative values from the maximum of volume variations. The initial isotropic pressure is equal to 500 kPa.

Figure 10 Simulation of q-constant loading paths for dense Hostun sand by the octo-linear constitutive model. The second order work is never vanishing.

Figure 11 Simulation of q-constant loading paths for loose Hostun sand by the octo-linear and the non-linear constitutive model. Points are placed by other symbols when the second order work takes negative values from the maximum of volume variations. The initial isotropic pressure is equal to 100 kPa.

Figure 12 Configurations of the slope and loading programmes to induce granular avalanches in a bi-dimensional medium.

Figure 13 Illustrations of the non-penetrability condition 13(a) and of the coulombian friction 13(b), where R_n and R_t are respectively the normal and tangential components of the interaction force and μ the friction coefficient. δ is the "distance" (roughly) between two grains and U_t the tangential inter-granular displacement.

Figure 14 Field of numerical incremental displacements at different values of rotation angle α.

Figure 15 Spatial comparison between negative values of second order work d^2W (on the left) and the values of kinetic energy e_c (on the right).

Figure 16 Comparison between global second order work and global kinetic energy as functions of rotation angle α.

Figure 17 Field of incremental displacements at different values of vertical plate displacement u.

Figure 18 Spatial comparison between the negative values of second order work d^2W (on the left) and the values of kinetic energy e_c (on the right).

Figure 19 Comparison between global second order work and global kinetic energy as functions of the vertical plate displacement.

Bibliography

Darve F., Labanieh S., 1982 "Incremental law for sands and clays. Simulations of monotonic and cyclic tests", Int. J. Num. Anal. Meth. in Geomech., 6 : 243-275

Hill R., 1967 "Eigenmodal deformations in elastic-plastic continua", J. Mech. Phys. Solids, 15 : 371-386

Rice J.R., 1976 "The localization of plastic deformation", Proceedings IUTAM Congress, 1 : 207-220

Vardoulakis I., Sulem J., 1995 "Bifurcation analysis in Geomechanics", Chapman & Hall publisher

Darve F., 1984 "An incrementally non-linear constitutive law of second order and its application to localization", in Mechanics of Engineering Materials, Desai and Gallagher eds, 179-196

Bigoni D., Hueckel T., 1991 "Uniqueness and Localization- I. Associative and Nonassociative Elastoplasticity",Int. J. Solids Structures, 28(2) : 197-213

Desrues J., 1990 "Shear band initiation in granular materials : experimentation and theory", in Geomaterials Constitutive Equations and Modelling, Darve ed., Elsevier, Taylor and Francis Books, 283-310

Darve F., Roguiez, X., 1998 "Homogeneous bifurcation in soils", in Localization and Bifurcation Theory for Soils and Rocks, Adachi et al. eds, Balkema publ., 43-50

Nova R., 1994 "Controllability of the incremental response of soils specimens subjected to arbitrary loading programmes", J. Mech. of Behav. Mater., 5(2) : 193-201

Hill R., 1958 "A general theory of uniqueness and stability in elastic-plastic solids", J. of the Mech. and Phys. of Solids, 6 : 239-249

Lyapunov A.M., 1907 "Problème général de la stabilité des mouvements", Annales de la faculté des sciences de Toulouse,9 : ,203-274

Chu J., Leong W.K., 2003 "Recent progress in experimental studies on instability of granular soil", Int. Workshop on Bifurcations and Instabilities in Geomechanics, Labuz et al. eds, Zwets and Zeitlinger publ., 175-192

Mandel J., 1966 "Conditions de stabilité et postulat de Drucker", Rheology and Soil Mechanics, J. Kravtchenko and P. M. Sirieys eds, Springer, Berlin, 58-68

Hermann H.J., Hovi J.P., Luding S., 1998 "Physics of Dry Granular Media", Kluwer Academic publ.

Bak P., 1996 "How nature works", Springer Verlag publ.

Drucker D.C., 1959 "A definition of stable inelastic material", J. Applied Mech., 26 : 101-186

Koïter W.T., 1969 "On the thermodynamic background of elastic stability theory",in Problems of Hydrodynamics and continuum Mechanics, SIAM, Philadelphia, 423-433

Chambon R., Desrues J., Hammad W., Charlier R., 1994 "CLoE, a new rate-type constitutive model for geomaterials. Theoretical basis and implementation", Int. J. Numer. Anal. Meth. Geomech., 18 : 253-278

Chambon R., Caillerie D., 1999 "Existence and uniqueness theorems for boundary value problems involving incrementally non-linear models", Int. J. Solids Structures, 5089-5099

Darve F., Chau B., 1987 "Constitutive instabilities in incrementally non-linear modelling", in Constitutive Laws for Engineering Materials, ed. C.S. Desai, Elsevier publ., 301-310

Darve F., Laouafa F., 2000 "Instabilities in Granular Materials and Application to Landslides", Mech. Cohes. Frict. Mater., 5(8) : 627-652

Darve F., Laoufa F., 2001 "Modelling of granular avalanches as material instabilities", in Bifurcation and Localization in Geomechanics, Muehlhaus et al. eds, Zwets and Zeitlinger publ., 29-36

Laouafa F., Darve F., 2001 "Modelling of slope failure by a material instability mechanism", Computers and Geotechn., 29 : 301-325

Darve F., Flavigny E., Méghachou M., 1995 "Yield surfaces and principle of superposition revisited by incrementally non-linear constitutive relations", Int. J. Plasticity, 11(8) : 927-948

Joer H., Lanier J., Desrues J., Flavigny E., 1992 "$1\gamma 2\varepsilon$: A new shear apparatus to study the behavior of granular media", Geotechn. Testing J., 15(2) : 129-137

Darve F., Laouafa F., Servant G., 2003 "Discrete instabilities in granular materials", Italian Geotechn. J., 37(3) : 57-67

Moreau J.J., 1994 "Some numerical methods in multibody dynamics, application to granular materials", Eur. J. Mech A., 13(4) : 93-114

Lanier J., Jean M., 1994 "Experiments and numerical simulations with 2D-disks assembly",Powder Technology, 109 : 206-221

Cundall P.A., Strack O.D.L., 1979 " A discrete numerical model for granular assemblies", Geotechnique, 29(1) : 47-65